Development of Mn/Cu Bi-Metallic MOF for Electrochemical CO₂ Reduction into Valuable Products

By

Umar Raza

Reg. No. 362683

Session 2021-23

Supervised by

Prof. Dr. Naseem Iqbal

A Thesis Submitted to U.S.-Pakistan Center for Advanced Studies in Energy

in partial fulfillment of the requirement for the degree of

MASTER of SCIENCE in

ENERGY SYSTEMS ENERGY

THESIS ACCEPTANCE CERTIFICATE

Certified that final copy of MS/MPhil thesis written by **Mr. Umar Raza** (Registration No. 362683) of US-Pakistan Center for Advanced Studies in Energy (USPCAS-E) has been vetted by undersigned, found complete in all respects as per NUST Statues/Regulations, is within the similarity indices limit and is accepted as partial fulfillment for the award of MS/MPhil degree. It is further certified that necessary amendments as pointed out by GEC members of the scholar have also been incorporated in the said thesis.

Signature: _____

Name of Supervisor: Dr Naseam Iabal

Date: 09/11/2023

Signature (HoD): _____

Date: 12/9/2023

Signature (Dean/Principal): _____

Date: 12/09/2623

I

Certificate

This is to certify that work in this thesis has been carried out by **Mr. Umar Raza** and completed under my supervision in Synthesis and Energy Storage laboratory, US-Pakistan Center for Advanced Studies in Energy (USPCAS-E), National University of Sciences and Technology, H-12, Islamabad, Pakistan.
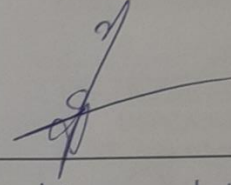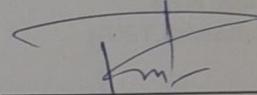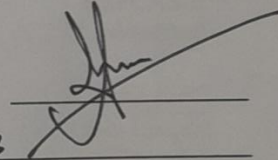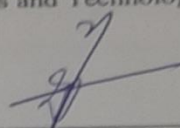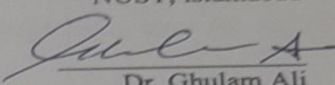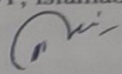
Supervisor:
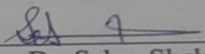
Dr. Naseem Iqbal
USPCAS-E
NUST, Islamabad

GEC member 1:
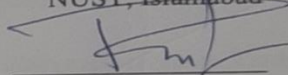
Dr. Ghulam Ali
USPCAS-E
NUST, Islamabad

GEC member 2:
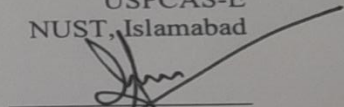
Dr. Nadia Shahzad
USPCAS-E
NUST, Islamabad

GEC member 3:

Dr. Sehar Shakir
USPCAS-E
NUST, Islamabad

HOD-ESE

Dr. Rabia Liaquat
USPCAS-E
NUST, Islamabad

Dean/Principal:

Dr. Adeel Waqas
USPCAS-E
NUST, Islamabad

II

Acknowledgments

First and foremost, I am thankful to Almighty ALLAH who is the creator and author of knowledge. Indeed, without YOUR blessings, this mammoth task would not have been possible. And I acknowledge that without YOUR willingness and guidance, I would not have done a single task.

I am grateful to my parents for their unconditional love and sacrifices. I am forever in your debt for your encouragement, financial and moral support. Thank you for keeping confidence in me. I profusely thank my Sisters for their immense support morally, always being there for me and cheering me up whenever I was down.

Dr. Naseem Iqbal, I express my sincerest gratitude to you for this opportunity, for your teaching, mentorship, and patience throughout the research. It has been truly a privilege to work with you. I would like to thank my GEC members **Dr. Nadia Shahzad, Dr. Sehar Shakir,** and **Dr. Ghulam Ali** for their guidance and help throughout my research.

 I am also thankful to the staff of Synthesis and Energy Storage Lab especially **Engineer Naveed** who helped in my research and gave valuable advice during my experimentation. I am also grateful to the other lab staff, faculty members, and administration who were a part of this journey. Also all my friends for their support both academically and in general.

And to life, an extraordinary experience with so many things to enjoy within a short span. Thank you for giving me so much in the years past, and for more to discover in the years to come.

Abstract

The development of affordable, functional, as well as highly discerning catalysts is of vital relevance to enhance the electrochemical reduction of CO_2 into useful products and chemical feedstock and to reduce excessive carbon dioxide emissions in the atmosphere. In this study, a novel electro-catalyst made of MnO and CuO nanoparticles fixed on Mn:Cu (1:2)@MOF is presented. The impressive current density of nearly $-58mAcm^{-2}$ at -2 V vs. Ag/AgCl (reference electrode) in 0.1M aqueous $KHCO_3$ electrolyte with nearly 54% faradic efficiency of methane and 52% of CO using two compartments H-cell is the result of these nanocomposites multiple active sites for electro-chemical carbon dioxide reduction. This performance stands in stark contrast to the Mn:Cu(1:1)@MOF and Mn:Cu(2:1)@MOF, which, under equivalent cathodic voltages, exhibit current densities of $-56mAcm^{-2}$ and $-51mAcm^{-2}$, respectively. The outstanding catalytic performance is attributed to the interaction of nanoparticles with MOFs, which enables improved CO_2 molecule absorption and activation due to accessible metallic components and unrivaled 2-D creation of Mn:Cu(1:2)@MOF. These findings offer a simple method for converting CO_2 into worthwhile goods using an analytical MOF alloy composition.

Table of contents

List of Figures

List of Tables

Chapter 1 Introduction

1.1 Energy and climate change

Non-renewable energy is produced using depletable resources and cannot be replenished within our lifetimes or for many generations. Fossil fuels like coal, petroleum, and natural gas, which developed millions of years ago from ancient plants and animals, represent the majority of non-renewable energy sources. Fossil fuels release harmful pollutants when burned, upsetting the balance of carbon in the environment and contributing to global warming. While fossil fuels are valuable for their energy content and accessibility, their extraction and use have significant environmental drawbacks [1]. Fossil fuels currently account for 80 percent of the global primary energy demand, while the energy system is responsible for approximately two thirds of global CO_2 emissions. Considering that methane and other short-lived climate pollutants (SLCPs) are likely to be significantly underestimated, it is probable that energy production and consumption contribute to an even larger portion of emissions. Moreover, a substantial amount of biomass fuel is presently utilized for small-scale heating and cooking purposes worldwide. These practices are highly inefficient and polluting, particularly when it comes to indoor air quality in many less-developed nations. The utilization of renewable biomass in such a manner poses a challenge to sustainable development [2]. Carbon dioxide levels in the Earth's atmosphere have risen to 412 parts per million (ppm) and continue to rise. This marks a 47% surge since the onset of the industrial era, when concentrations were around 280 ppm. Additionally, there has been an 11% increase since 2000, when concentrations were approximately 370 ppm [3]
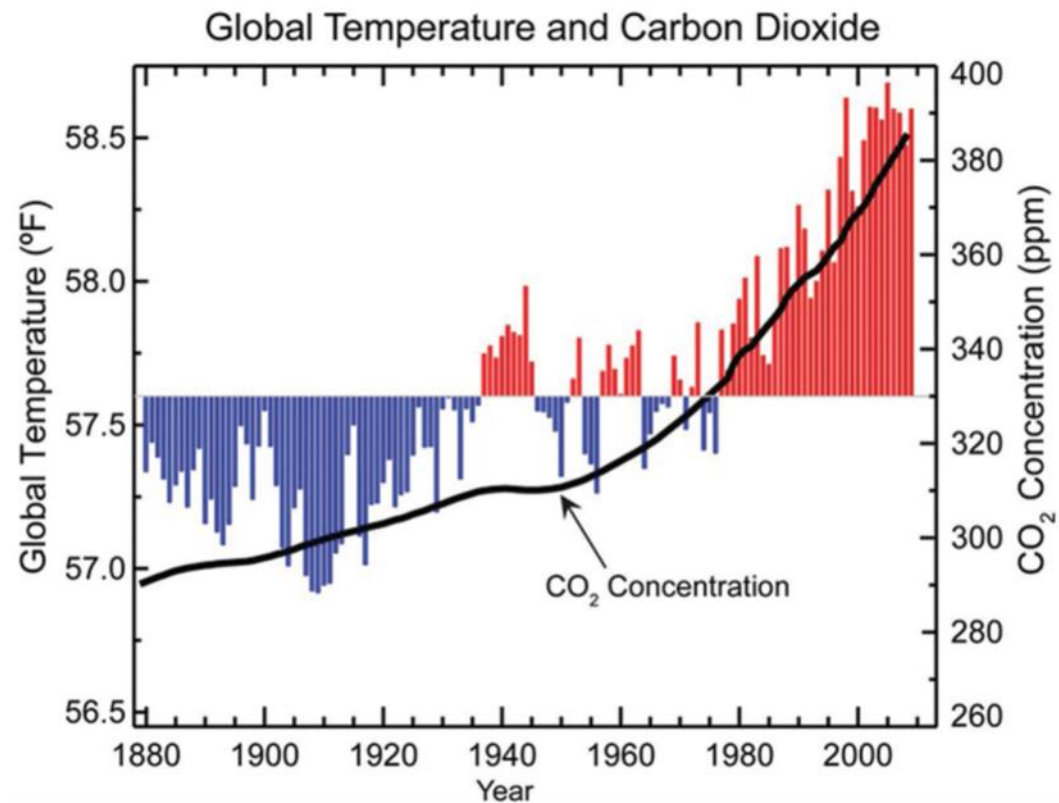
Figure 1.1: Graph showing the CO_2 concentration in the atmosphere and equivalent universal average temperatures since the 19th century [4].

An energy system of the future must possess resilience and adaptability to effectively withstand the unavoidable consequences of climate changes, including droughts, heat waves, and storms. It is widely recognized that there is a positive correlation between growth and energy. As economies expand, the demand for energy, particularly from fossil fuels, also increases. However, renewable energy sources offer an environmentally friendly and low-carbon alternative. Renewable energy sources such as solar, wind, geothermal, and hydroelectric power generate clean energy devoid of greenhouse gas (GHG) emissions. In recent years, many countries have embraced renewable energy technologies as a means to safeguard the environment. Furthermore, several factors, including energy supply security, energy dependency, climate change, energy price volatility, health concerns, and environmental disasters, have prompted emerging economies to shift towards renewable energy sources. Economists, governments, policymakers, and researchers are actively

seeking methods to ensure a sustainable and healthy environment for future generations [5].
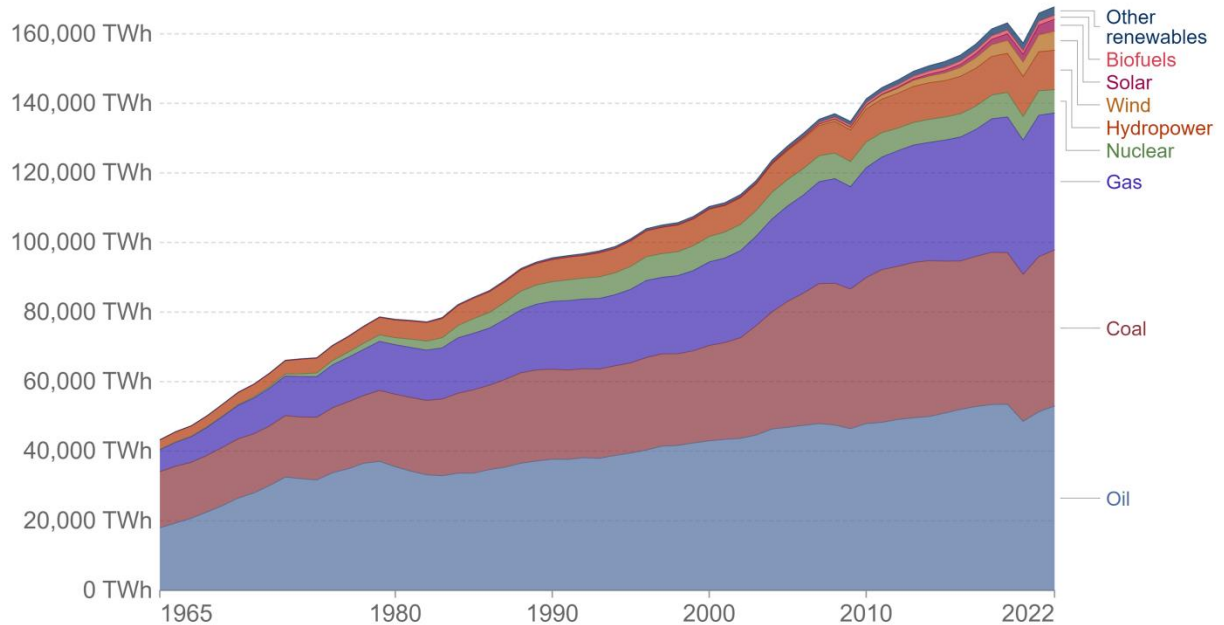
Figure 1.2 World Energy Consumption scenario [6]

1.1.1 Carbon Capture, Utilization and Storage (CCUS)

Carbon capture, utilization, and storage (CCUS) encompasses the process of capturing CO_2 emissions, typically originating from significant point sources such as power plants or industrial complexes fueled by fossil fuels or biomass. Once captured, the CO_2 is compressed and conveyed via pipelines, ships, railways, or trucks for utilization in various applications or injected into deep geological formations like depleted oil and gas reservoirs or saline aquifers [7]. There are several ways for clean energy transition using CCUS technology, such as

1. **To address emissions from the current energy infrastructure**, the retrofitting of Carbon Capture, Utilization, and Storage (CCUS) technology to existing power and industrial plants offers a viable solution. This approach effectively mitigates the potential release of 600 billion tons of CO_2 over the next five decades.

2. **Addressing some of the most daunting emissions challenges**, heavy industries presently contribute to nearly 20% of the global CO_2 emissions. Among various technological solutions, CCUS (Carbon Capture, Utilization, and Storage) stands out as the primary means for achieving significant reductions in emissions originating from cement production. Moreover, it proves to be the most economically viable approach in numerous regions for curbing emissions in the realms of iron and steel manufacturing, as well as chemicals production. The captured CO_2 plays a vital role in the supply chain of synthetic fuels derived from CO_2 and hydrogen—a limited selection of low-carbon alternatives, particularly for long-distance transportation, including aviation.

3. **An economically efficient route for generating low-carbon hydrogen.** CCUS enables the swift expansion of low-carbon hydrogen production to fulfill existing and future requirements arising from emerging applications in transportation, industry, and buildings.

4. **Removing carbon from the atmosphere** CCUS represents an essential technology strategy for extracting carbon and creating a net-zero energy system for emissions that cannot be prevented or reduced directly. [8].
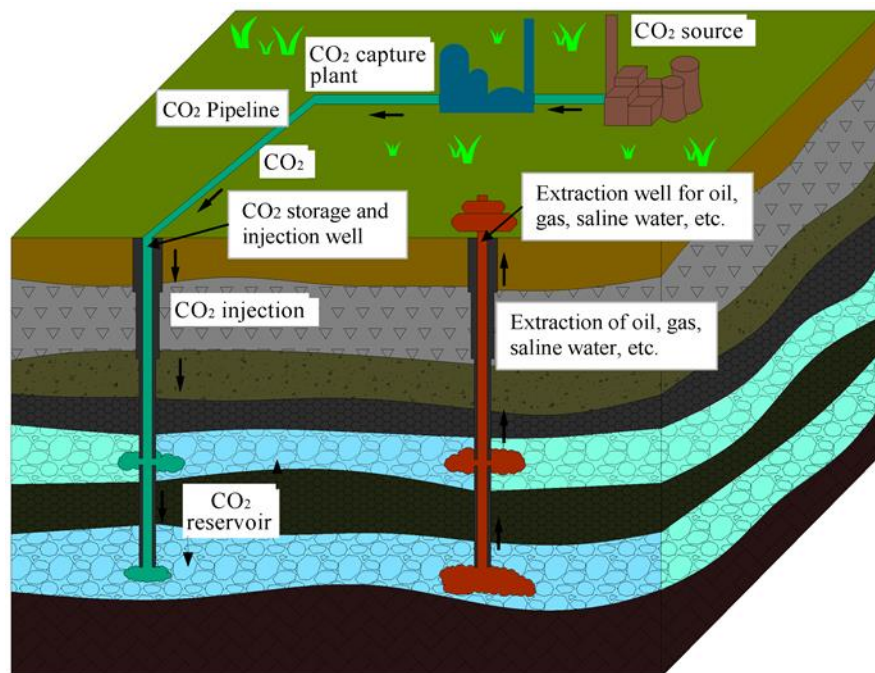
Figure 1.3 Model for carbon capture and storage [9].

1.1.2 Carbon Dioxide Reduction

The CO_2 reduction to other chemicals can be done by different methods such as thermochemical, photochemical, and electrochemical pathways. The choice of catalysts and process technology is very crucial as it heavily depends on the methods employed. For example, the catalysts should be stable at higher temperature in a thermochemical reaction, the catalyst should able to minimize the competitive H_2 evolution reaction expected in the electrochemical method, and an appropriate semiconductor with a minimum band gap of 1.23 eV is required for the photochemical method[10].
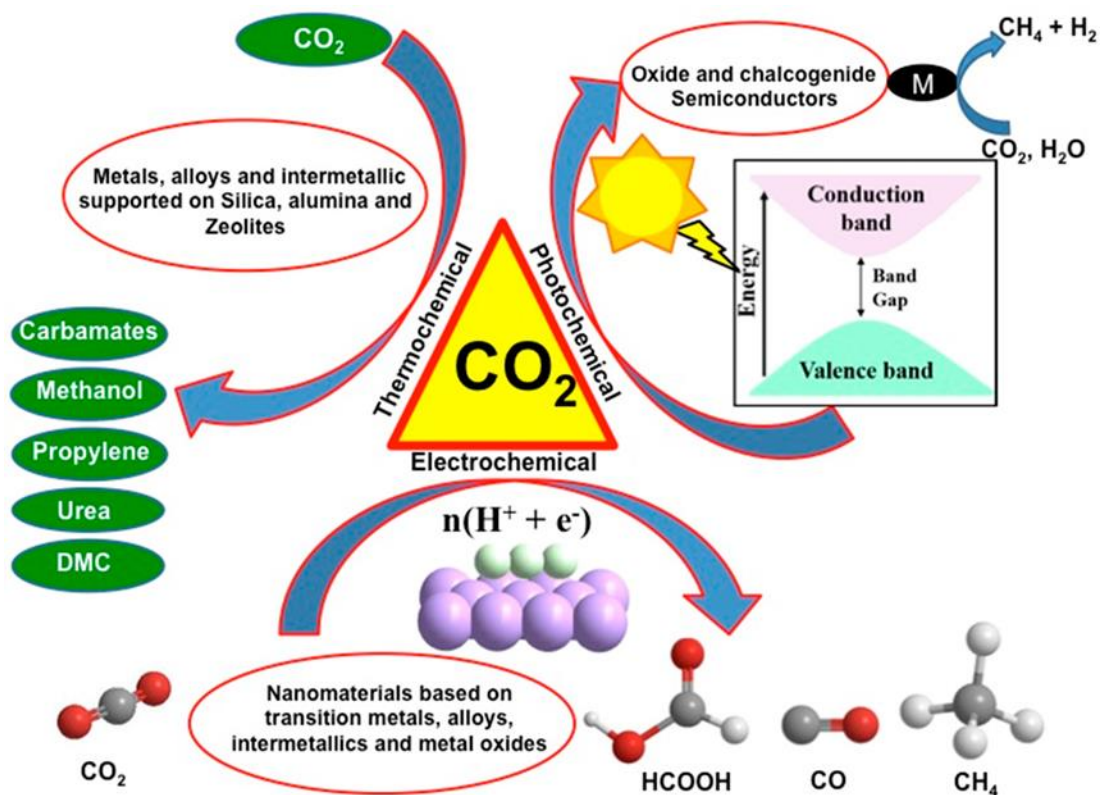
Fig 1.4 Different ways of CO_2 reduction[10]

1.2 Photosynthesis

Photosynthesis is a very important natural phenomenon in which plants and trees absorb CO_2 and utilize sunlight to convert that CO_2 into oxygen and carbohydrates[11].

It mainly consists of two reactions:

• **Light reaction**: In this reaction, the plant absorbs sunlight through chlorophyll and converts it into chemical energy, and stores it while oxidizing water into O_2.

• **Dark reaction**: During this process, the energy stored is used to convert CO_2 absorbed from the atmosphere by plants to carbohydrates[12].

1.3 Synthetic Photosynthesis

Extensive research has been conducted over an extended period to gain a comprehensive understanding of the photosynthesis process. This knowledge has paved the way for the development of artificial photosynthesis techniques in laboratories, eliminating the reliance on plants. The aim is to efficiently convert a larger amount of CO_2 into valuable fuels by harnessing sunlight as the primary energy source. However, the current efficiency levels of artificial photosynthesis fall significantly short of meeting the demands for commercial applications. Currently, two approaches are employed to tackle this challenge:

1.3.1 Photocatalysis by Indirect Light

In this particular method, photovoltaic (PV) cells are employed to absorb sunlight and produce photo voltage. This photo voltage is then directed to a two-electrode system. At these electrodes, electro catalysts play a crucial role in augmenting the speed and selectivity of the reaction. The primary advantage of this step lies in the flexibility it offers for designing the PV system and selecting appropriate electro catalyst pairs.

1.3.2 Direct Photocatalysis

The second approach utilizes direct absorption of sunlight by the semiconductor particles (photo catalysts) equipped with electro catalysts that work as a co-catalyst spread in aqueous solution and cause direct light-harvesting, charge transfer through all particles. The second route is much more compact and straightforward because of its wireless configuration. These two approaches provide an alternative route for natural photosynthesis and their efficiency is mainly dependent on the performance of their photo catalysts and electro catalysts.
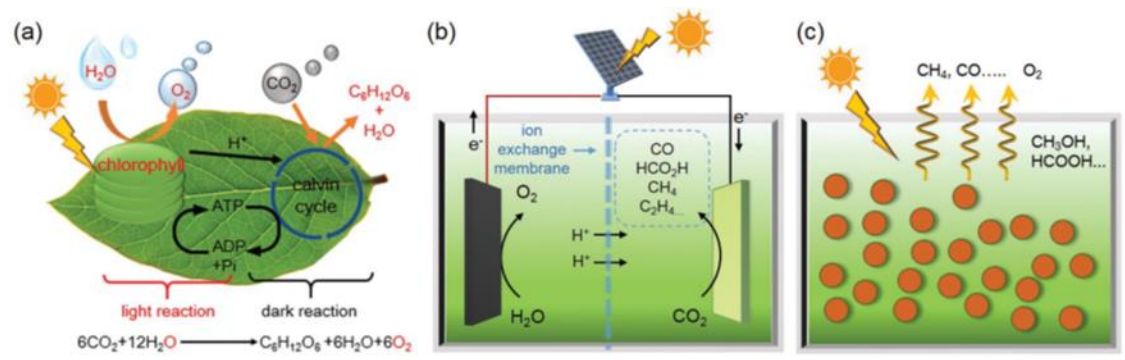
Fig. 1.5 Equivalence of photosynthesis, electrochemical synthesis on electro-catalysts powered by a photovoltaic cell, and photochemical synthesis on chemical powders (a), (b), and (c) [12]

1.4 CO$_2$ Reduction through Electrocatalysis

Electrochemical CO$_2$ reduction (CO$_2$R) is one of several promising strategies to mitigate CO$_2$ emissions. Electrochemical processes operate at mild conditions, can be tuned to selective products, allow modular design, and provide opportunities to integrate renewable electricity with CO$_2$ reduction in carbon-intensive manufacturing industries such as iron and steel making. In recent years, significant advances have been achieved in the development of highly efficient and selective electrocatalysts for CO$_2$R[13].

a) The reaction electrode potential and temperature may be easily regulated

 b) The electrolyte employed is infrequently used and easy to recycle

 c) Many renewable technologies, such as solar PV systems, can be used as an energy source to reduce CO$_2$ electrochemically; and

d) The electrochemical cell can be designed in a variety of ways.
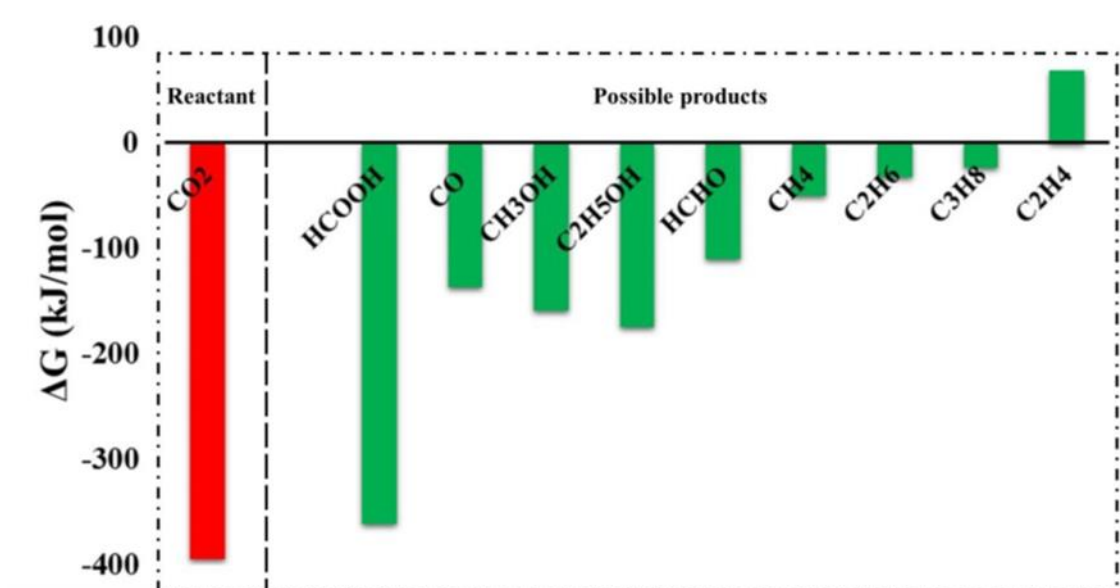
Fig. 1.6 CO_2 reduction chemical compounds with Gibbs-free energies are depicted in the graph [17].

1.5 Electro-catalytic CO_2 Reduction Basics:

During the process of electrocatalytic CO_2 reduction, electrons flow from the anode to the cathode, leading to the reduction of CO_2 at the cathode. To generate a voltage across two electrodes, an external electrical source provides the necessary energy. An aqueous medium or electrolyte acts as an ion carrier, facilitating the movement of ions between compartments through a membrane. At the anode, water is oxidized, releasing electrons and H+ ions that aid in the hydrogenation of CO_2. Figure 1.8 depicts the procedure for converting CO_2 to CO, which is a straightforward electron transfer reaction requiring two electrons [17].
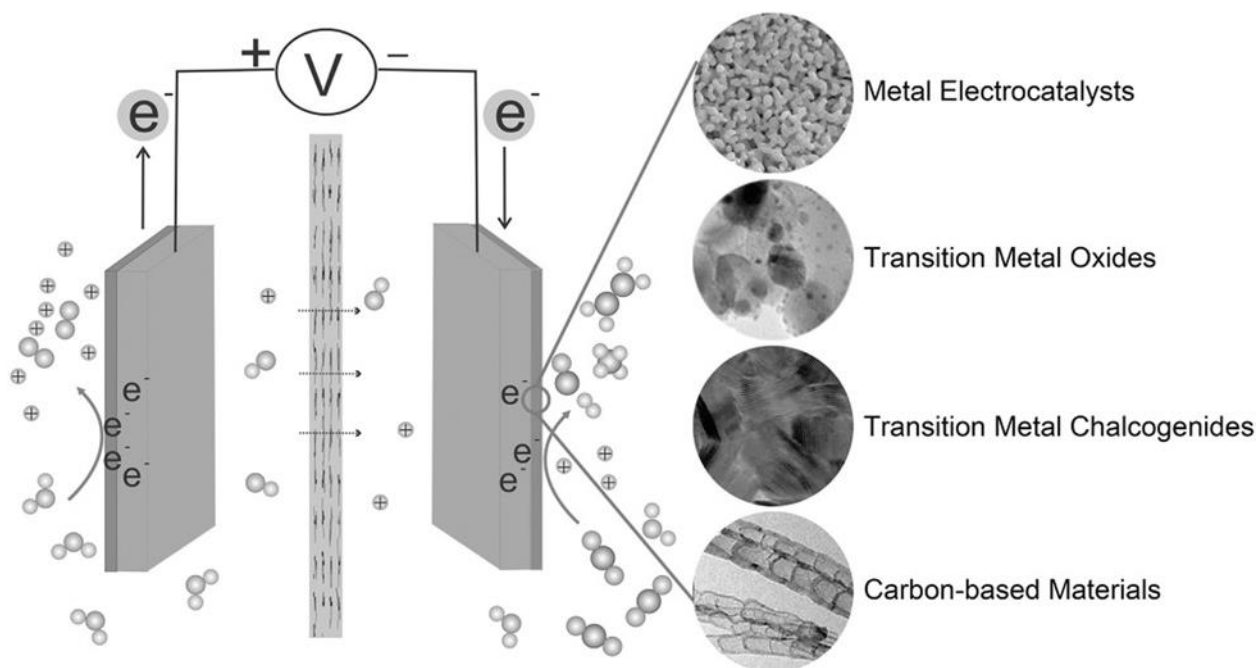
Fig 1.7 Diagram of a reaction unit and four types of catalysts used in electrochemical CO_2 reduction [14]
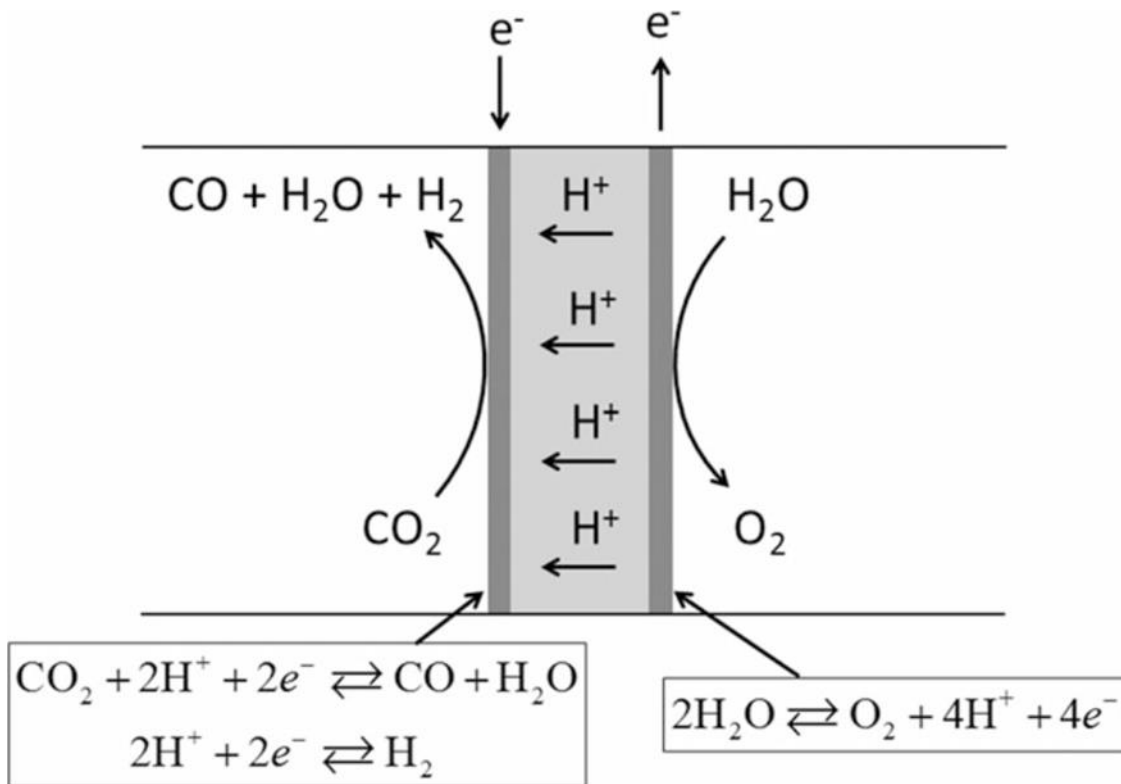
Fig 1.8 Electrolyte-containing cell with a cation-exchange membrane (CEM).The model is similar to that of a proton-exchange membrane fuel cell [17].

Here, the water is split at the anode to produce O_2, and the released electrons go through an external circuit to the cathode, where they convert CO_2 to CO. In the cathode reaction transfer over the CEM (cation exchange membrane), the two hydrogen ions are shown. The proton exchange membrane fuel cell design and the above design are quite similar.

1.5.1 Electroreduction of CO_2 to methanol

Another illustration involves the transfer of at least six electrons, which calls for a high voltage and energy, in order to convert CO_2 to CH_2OH. To illustrate the reaction taking place on the anode and cathode, Potentials are displayed in relation to a saturated calomel electrode.

Electrode Reactions:

Cathode: $CO_2 + 6H^+ + 6e^-$ $CH_3OH + H_2O$, $E^0 = -0:22$ V

Anode: $3H_2O$ $1.5O_2 + 6H^+ + 6e^-$, $E^0 = +0:99$ V

10

Overall: $CO_2 + 2H_2O$ $CH_3OH + 1.5O_2$, $E^0 = +1:21$ V
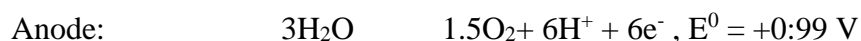
According to above equation, the reaction requires six electrons and hydrogen ions, which complicates and presents a challenge in terms of energy (Figure 1.9) [17]. Although research has been done on the design of catalysts for the conversion of CO_2 to methanol, the conversion efficiency and selectivity are rather quite poor. However, from an economic perspective, noble metals like platinum that may successfully trigger this reaction are highly costly. In order to minimize the energy barrier for this reaction while simultaneously making it relatively affordable and accessible, research has been focused on the creation of a catalyst. Recently, it has been shown that copper metal, its oxides, and composites are particularly efficient in converting CO_2 into methanol.
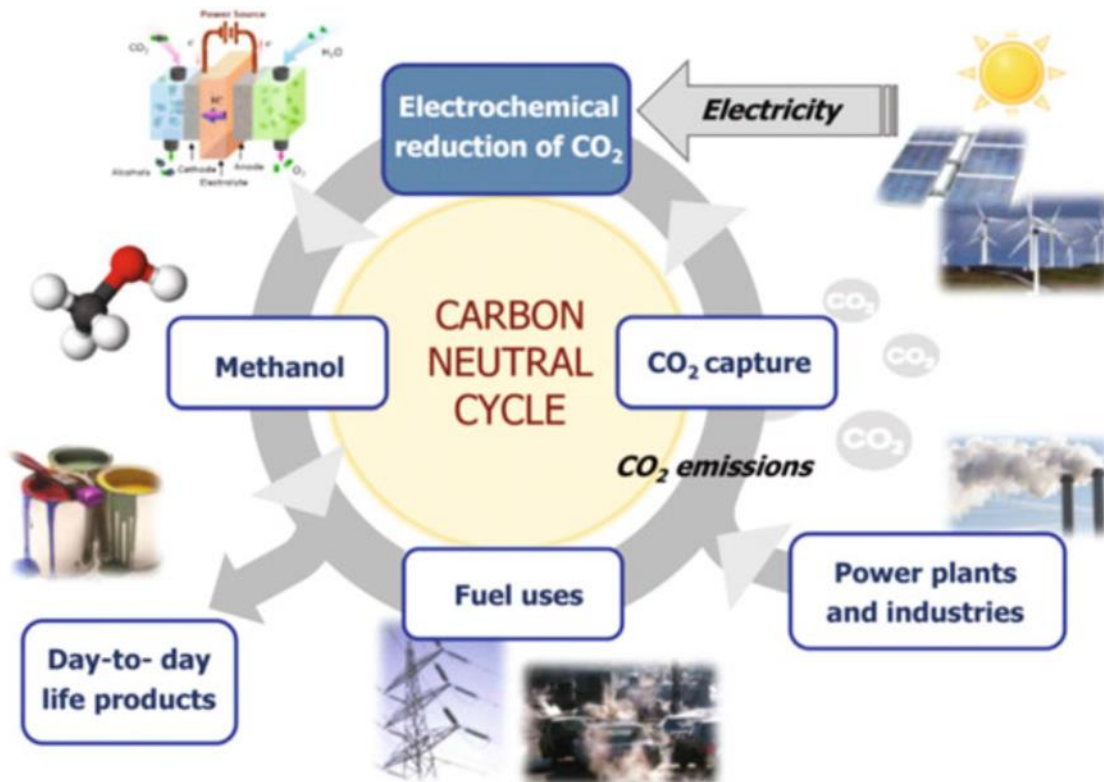
Fig 1.9 Economic cycle model based on methanol [17]

1.6 Water splitting and reduction of CO_2

Water splitting and the electrocatalytic reduction of CO_2 are not that dissimilar from one another. A photocatalyst of the semiconductor kind is employed while splitting or reducing water. The

primary byproduct of this reaction is H_2. As a result, at 25°C and pH = 14, the CO_2 reduction reaction and the thermodynamically possible H_2 production reaction compete with one another:

$CO_2 + H_2O + 2e^-$ $HCO_2^- + OH^-$ $E^0 = -1{:}02$ V

    $2H_2O + 2e^-$ $H2 + 2OH^-$ $E^0 = -0{:}83$ V
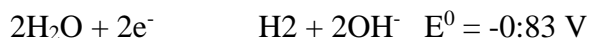
In order to produce voltage, electrical energy will be required in two opposing conversion processes: the creation of H_2 by water splitting and the conversion of CO_2 into the desired product, such as formic acid or methanol. Reduce hydrogen formation so that all the energy is used in the reaction of CO_2 reduction, and you may obtain high selectivity of the desired product or high faradaic efficiency of the necessary product. The equilibrium potentials (vs. SHE) of several products formed by CO_2 reduction in pH 7.0 aqueous solution are reviewed in Figure 1.10 [16].

Reduction potentials of CO_2	$E°$ [V] vs SHE at pH 7
$CO_2 + e^- \rightarrow CO_2^-$	−1.9
$CO_2 + 2H^+ + 2e^- \rightarrow HCOOH$	−0.61
$CO_2 + 2H^+ + 2e^- \rightarrow CO + H_2O$	−0.52
$2CO_2 + 12H^+ + 12e^- \rightarrow C_2H_4 + 4H_2O$	−0.34
$CO_2 + 4H^+ + 4e^- \rightarrow HCHO + H_2O$	−0.51
$CO_2 + 6H^+ + 6e^- \rightarrow CH_3OH + H_2O$	−0.38
$CO_2 + 8H^+ + 8e^- \rightarrow CH_4 + 2H_2O$	−0.24
$2H^+ + 2e^- \rightarrow H_2$	−0.42

Fig 1.10 Standard electrode potentials for various CO_2 reduction products [15]

1.7 Reaction Mechanisms for various Products

This topic discusses the kinetics of CO_2 reduction and several reaction pathways. Some processes are more advantageous because carbon dioxide is a fairly stable molecule, while other reduction reactions have slower and more intricate kinetics than the two-electron hydrogen evolution reaction. This is so that a bent radicle ion may develop in the initial phase of the production of the

CO_2 radicle, which needs a high voltage of -1.9 V to do so. Typically, this stage is referred to as the rate-determining step.

Two actions could be taken to reduce this CO_2 −:

• The hydrogen ion protonates its oxygen atoms to generate the intermediate COOH, which undergoes conversion to CO and yields the desired product.

• By adding a proton to the carbon atom of or at a high potential, HCOO is produced, which is then reduced once more to yield $HCOO^-$ (formate).

Owing to their high energy barrier, very few materials, such as copper, are capable of reducing CO_2 to hydrocarbons. Despite being difficult to understand, the reactions are thought to happen by H addition, C-O bond scission, and C-C bond coupling. These chemical pathways are shown in Figure 1.11 [17].
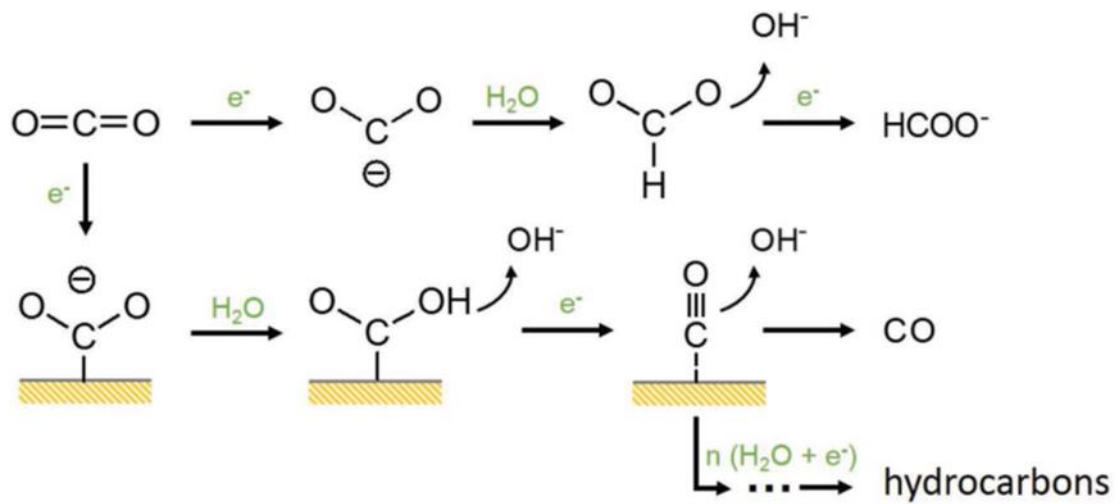
Fig 1.11 Possible electrocatalytic CO_2RR reaction routes in aqueous solution on metal electrodes are depicted. Permission granted for modification [16].

1.8 Electrocatalytic CO_2 Reduction Methods

These are two broad categories of electrocatalytic CO_2 reduction processes:

• Homogenous catalysis

• Heterogeneous catalysis.

1.8.1 Homogenous Catalysis

For the Electroreduction of CO_2, a wide range of molecular materials and compounds are often utilized. As illustrated in Figure 1.12, they function as an electron charge transferor between the electrode surface and CO_2 to enable indirect electrolysis to take place [17]. The potential necessary for a homogeneous catalyst to decrease CO_2 and a direct reduction of CO_2 is different. Because of this, the voltage for direct CO_2 conversion is lower than the potential for CO_2 homogeneous catalysis. Every material has specific characteristics that must be present for them to function as homogeneous catalysts, such as an appropriate reduction potential, high reduced catalyst stability, and a high degree of reaction obtained from the catalyst in order to obtain a large amount of yield quickly.

1.8.2 Heterogeneous Catalysis

The kind of product created and the volume of product produced depend on the energy of binding between the electrode surface and the CO_2 molecules and intermediates. The heterogeneous catalysis is seen in Figure 1.12. The quantity of reaction intermediate that will be adsorbed to the catalyst surface and affect the reaction capacity depends on the surface area of the specific catalyst. Now that materials with nanostructures have a greater surface area to volume ratio, they are inherently more suited to reducing carbon dioxide at higher rates. Due to their capacity to create composites and nanostructure, heterogeneous materials are more reliable in this situation than single molecules since they have more features to offer as a catalyst for greater CO_2 reduction. It is possible to more efficiently regulate trash, separate products, and reuse the stream in a flow cell during the heterogeneous catalyst process.

1.9 Catalyst material

Depending on the kind of reaction, a catalyst material may be a metal, semiconductor, metal oxide, metal halide, organic molecule, or organo-metal. This substance aids in accelerating the reaction's pace and enhancing the selectivity of a desired outcome. The catalyst material is either produced or can be purchased in its purest form from the market. It is applied to the cathode's surface using a pipette to drop coat ink, among other methods, to create a layer on the electrode's surface, which in most cases is a glassy carbon electrode.
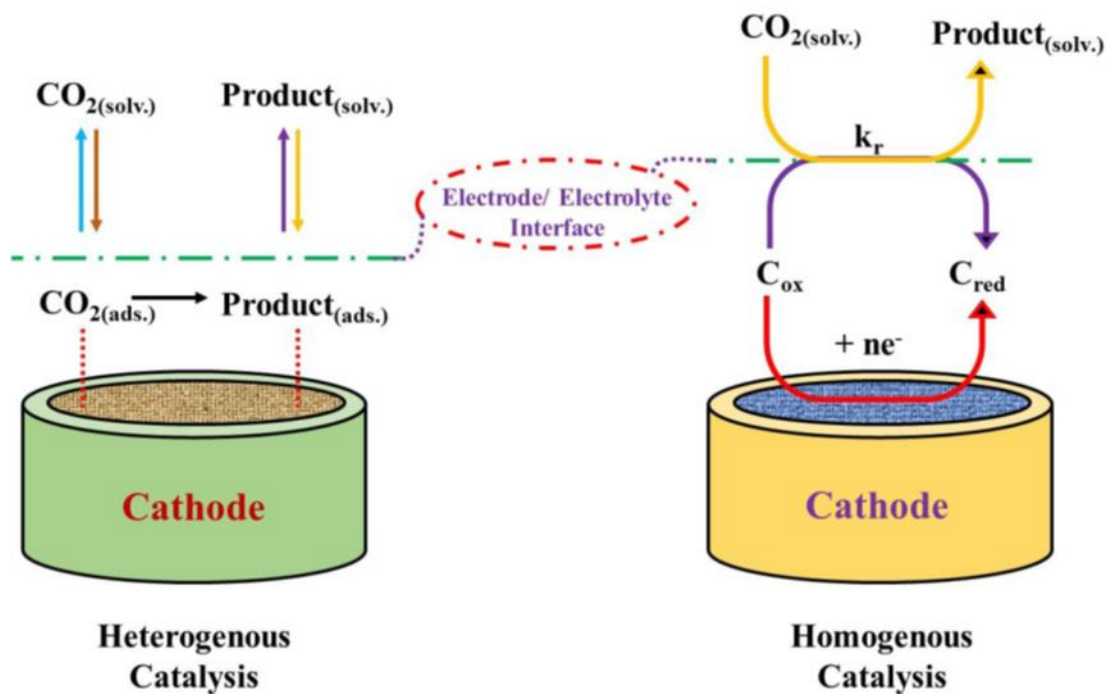
Fig 1.12 Heterogeneous and homogenous catalysis are shown schematically [17].

1.9.1 Pt modified N-doped Graphene

A costly noble metal with a very high catalytic activity is platinum. Due to the high cost of using pure Pt, it is typically doped with more affordable and useful elements. The methanol F.E of the Pt modified N-doped graphene at -0.30V (vs. Ag/AgCl) was 41%. It was found that the H_2 atoms on the surface of Pt changed when pyridinium ion was produced as a proton was taken by the pyridine in N-graphene. Hydrogen atoms in the form of *COOH are electrophilically attacked by the CO_2 molecules. The intermediate interacted with PyH^+ to produce PyH^+...COOH, which reduced to produce methanol [19, 20].

1.10 Challenges and Restrictions in Electro-catalytic CO_2 reduction

Thermodynamics and kinetics are the two main restrictions to electrocatalytic CO_2 reduction. Compared to its conversion into more desired compounds like methanol, methane, and formic acid, the reduction of CO_2 into CO is simpler. Multiple electron transfers are necessary for the formation of methanol, which raises the energy barrier or kinetics needed for the reaction and reduces its total productivity. Lowering the energy cost of the reaction and improving the

selectivity of the intended product can both be aided by the discovery of an ideal electrocatalysts that can encourage the transfer of more electrons at low voltage. In order to create a catalyst with the needed diversity of properties, many catalysts might be mixed.

1.10.1 Electrode Over-potential

It is described as a shift in the electrode potential relative to the applied thermodynamic potential. It is a significant obstacle to reducing carbon dioxide. Three elements make up the over-potential.

1. **Ohmic over-potential:** Electrolyte and electrode resistances are responsible for the ohmic losses.

2. **Activation over-potential:** The kinetic limit, or the amount of energy required to maintain the electrode reaction at a significant level, is shown by the activation over-potential.

3. **Concentration over-potential:** The restriction in mass transfer caused by the diffusion of products and reactants towards/away from the electrode surface leads to the development of the concentration over-potential.

The diffusion rate is extremely low since the CO_2 conversion takes place in an aqueous medium at low temperatures. The current flow will be minimal if less CO_2 reaches the electrode's surface than is consumed since there won't be enough CO_2 for the electrons to decrease. So long as the CO_2 flow rate is maintained, the electrochemical cell will continue to experience a steady reaction. The low solubility of carbon dioxide in water, which is around 30 mmol L-1 (at 293K and 101 kPa) presents another difficulty. The effectiveness of our reaction is constrained by the fact that it dissolves less readily in aqueous electrolytes than in water [17]. To maintain the concentration of CO_2, pre-absorption procedures such as purging the electrolyte for 30 minutes before conducting the reaction might be utilized [18].

The design should be compact and effectively sealed because if the cell sealing leaks, it will automatically release CO_2 and other significant product gases from the cell, diminishing efficiency. The effectiveness of cells and our response are also influenced by the sort of membrane used. A high-quality porous Nafion membrane improves the exchange of ions between chambers in a cell. It should be carefully recycled to get rid of any pollutants or blockages that can prevent

it from functioning correctly. Overall, designing an electrochemical cell is difficult. Thus it is essential to choose parameters compatible with the demands of the required reactions.

1.11 Reason/Justification for the Selection of the Topic

The main goal of this research is to create an efficient CO_2 electrochemical reduction catalyst that has high performance (high faradaic efficiency, high current density), affordable, and extremely long-lasting. The daily rise in atmospheric carbon footprints is a significant problem for nations with substantial industrial CO_2 emissions. We observe several emerging technologies attempting to recycle CO_2 in a world under pressure to keep global temperature rises to below 20C. Their scope spans from methods being explored at the lab scale to ones that are close to commercialization, such electrocatalytic reduction. The most important methods to effectively utilize CO_2 and lessen its impacts have been carbon capture and reduction. There have been several reports of both homogeneous and heterogeneous catalysts in the literature, and they all show promise for CO_2 reduction. Because they are far more affordable than noble metals and exhibit excellent efficiency like noble metals, heterogeneous catalysts have been the subject of extensive experimentation. The superb selectivity toward usable hydrocarbons, high stability, durability, and effectiveness towards CO_2 reduction of Mn:Cu@MOFs nanomaterial has been presented. This will be a significant effort to use up extra carbon in the atmosphere and help increase fuel resources in addition to lowering global warming.

1.12 Problem statement

Incomplete CO_2 reduction due to catalytic instability, its sluggish kinetics and improper current density .Unstable catalysts, sluggish reactions, and insufficient electrical current levels hinder the conversion of useful products. We require stable catalysts, quicker reactions, and the proper current density to enhance CO_2 reduction. This facilitates the efficient conversion of CO_2 into useful goods, assisting in the fight against climate change.

1.13 Objectives

- To synthesize and test electrocatalyst for CO_2 reduction with high current density and selectivity.

- To Characterizing Mn:Cu@MOFs catalysts based on copper and manganese doping using a solvothermal method.
- To analyze results of products obtained from electrochemical CO_2 reduction.

1.14 Adaptability to National Needs

Pakistan's environmental situation is becoming more dangerous as it continues to deteriorate. As of 2014, Pakistan has 65,038 CO_2 emissions from gaseous fuel, and as automobiles and industries grow, that number will rise. According to Public Climate Expenditure of UNDP's and Institutional Review 2015, Pakistan would need to spend $10.70 billion year on adaptation costs over the next 40 years, and $8 to $17 billion annually on mitigation costs. Pakistan is the 33rd-largest CO_2 producer in the world, generating 171 $MtCO_2$ in 2015. These are more than simply facts; they present a problem that must be solved and a barrier that, in the absence of enough research and development, will only worsen. Utilizing and studying cutting-edge technology like carbon capture and CO_2 reduction, which will absorb and transform that carbon into valuable goods, is the only chance we have in this situation. Electricity, which is produced from a renewable resource, water, is used in electrochemical CO_2 reduction. The invention and production of the catalyst utilized in that reduction process represents the main challenge of this research. An efficient catalyst will aid in the process' improvement and boost its commercialization, allowing CO_2 to be removed from the environment and converted into hydrocarbons that can be utilized in cars, increasing fuel economy overall and lowering emissions.

1.14 Benefits & Application Areas

• One of the main problems facing the globe today is air pollution, which is being helped through CO_2 consumption and decrease.

• The transformation of carbon dioxide (CO_2) into usable hydrocarbons as methanol, ethanol, methane, etc.

• The production of additional chemicals and gases, such as acetic acid and formic acid, which serve as valuable solvents and carbon monoxide, which may be utilized to create syngas.

• Controlling global warming.

• The primary industry and sector for the application is transportation, which produces the most CO_2 emissions.

• This technique may become a commercial fuel source as fuel resources are decreasing.

Summary:

The primary problems with energy sources are covered in this chapter. The history of CO_2 emissions and the previous tactics and techniques for its reduction are explored. The most recent studies on CO_2 reduction were examined. The electro-catalytic CO_2 reduction process' primary step was introduced. Applications and the necessity for the research are discussed.

Chapter 2   Literature review

2.1 Catalysts employed in earlier studies

This section provides an overview of previously researched catalysts for electrochemical CO_2 reduction. Many different types of catalysts have been produced, including metals, metal oxides, metal-organic frameworks, metal chalcogenides, carbonates, and so on. Each of these materials has a distinct structure and response.

2.1.1 Metals

Many metals, including Bi, Sn, and in, have been used in this technique. This group is incapable of absorbing CO_2 or its intermediary CO, Desorbed CO_2 tends to be protonated at the carbon atom and transforms to formic acid or formate as the major reduction product. The second group of metals is relatively expensive and noble, such as Ag, Au, Pd, Zn, and others that have a high performance rate but are quite uncommon in nature. These metals attach the CO_2 intermediate, catalyze the breaking of the C-O bond to CO_2, and cause the resultant CO to appropriately desorb into an electrode product (Figure 2.1) [21]. Pt, Ti, Ni, Fe, and other metals are included in the third category. They have significant CO adsorption capabilities and a lower HER overpotential, resulting in H_2 as the primary product of CO_2 reduction. Among the three classes of elements, only the Cu metal produces large amounts of C1-C3 hydrocarbons. As previously researched, elemental metals are used as CO_2RR electrocatalysts. Hori et al. originally demonstrated that CH_4, CO, formate, and other hydrocarbons were sensed from the CO_2RR electrocatalytic on different metal cathodes in $KHCO_3$ aqueous electrolyte solution in a series of major papers published throughout the 1980s and 1990s [22].
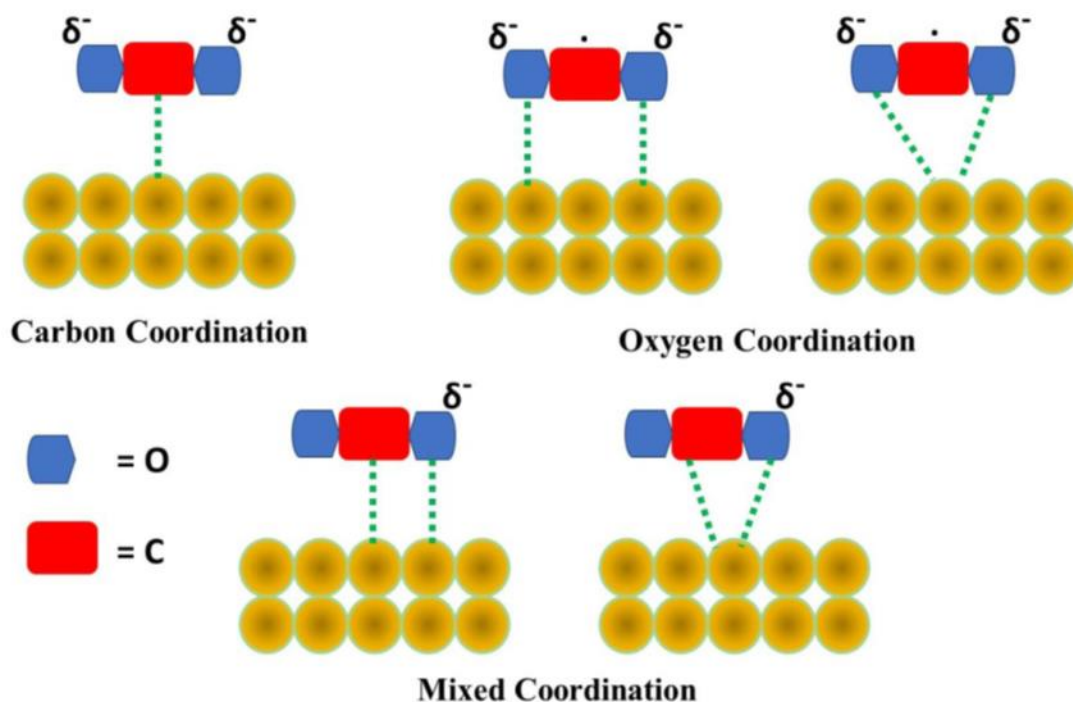
Fig. 2.1 Illustration showing the interaction of CO_2 with a metal surface [23]

2.1.1.1 Properties of Pd

Pd is another noble metal that is both expensive and extremely uncommon in nature. Its nanoparticles have been discovered to be highly catalytic. The electroreduction of CO_2 to carbon monoxide over Pd nanoparticles with diameters ranging from 2.4 to 10.3 nm demonstrated significant size-dependent performance and selectivity. Faradaic efficiencies range from 91.2% for 3.7 nm nanoparticles to 5.8% for 10.3 nm nanoparticles, with an 18-fold increase in current density [23].

2.1.1.2 Properties of Sn

Tin has previously been reported in the literature as having great activity and selectivity for converting CO_2 to formic acid and formate. Lee & al. obtained a faradaic efficiency of only 18% of formate by electrocatalysis while incorporating Sn particles on carbon paper, whereas Sridhar et al. obtained an F.E value of 80% by utilizing a comparable tin electrode. Kanan et al reported a faradaic efficiency of 58% for formate on tin/tin oxide electrodes compared to 19% for tin foil. CO_2 electrochemical reduction is followed by H_2 evolution in an aqueous solution; however, CO_2

conversion is simpler than H_2 evolution on Sn material at the cathode potential of 1.4 to 1.8 V vs. Ag/AgCl [26, 27].

2.1.1.3 Properties of Cu

Copper is the only metal catalyst that can reduce carbon dioxide beyond formate and CO to generate high carbon content hydrocarbons such as ethane, methane, methanol, ethylene, and ethanol, which have been documented and can be used as fuels. Alivisatos and colleagues reported an 80% methane production efficiency utilizing Cu NPs (7 nm, escalated to 25 nm via electrochemical testing) with a current density four times greater than Cu foil. Jianwei and colleagues employed a pressured (60 atm) supercritical CO_2 water mixture to produce methane over a Cu catalyst.

The firm binding of CO to the copper surface has suppressed HER. When CO is reduced in the presence of water, the intermediate formyl CHO is produced. Because of the adsorbed CO reduction, CHO*, CH_2O*, and CH_3O* are produced on the catalyst's surface .Cu catalysts aid in the hydrogenation of oxygen atoms in CH_3O* to create methanol. The electrocatalytic reduction pathway of CO_2 on the copper surface is depicted in Figure 2.2 [28]. Cu metal is not particularly stable and has a small surface area, but its ability to overcome the barrier for CO_2 conversion to higher carbon hydrocarbons makes it very important in improving the selectivity of the reduction process [8].
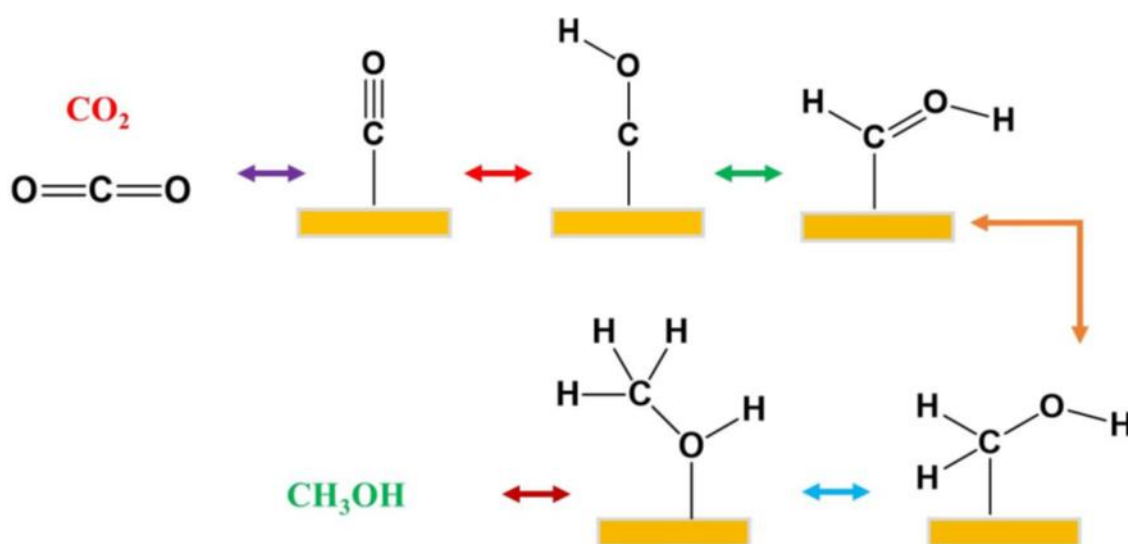
Fig 2.2 A schematic illustration of the procedure occurring on the surface of the Cu electrode [28]

2.1.1.4 Cu Electrode-based thick Cu_2O sheets

By annealing Cu foil in air and electrochemically decreasing the Cu_2O, modified Cu electrodes were created. The CO_2 conversion of these electrodes was strongly dependent on the main thickness of the Cu_2O layer [29]. Electrodes were created by annealing Cu_2O layers at 130°C, whose functionalities were identical to polycrystalline Cu. A combination of these features at low overpotentials resulted in a current density of >1 $mAcm^{-2}$ in CO_2 reduction.

2.1.1.5 Nanocatalysts made of copper selenide

This is a Copper metal and Selenide alloy. Selenide is not a metal. It is similar to arsenic. It is rarely found in its elemental form or as pure ore complexes beneath the Earth. It is found mostly in metal sulfide ores. This composite has demonstrated excellent activity toward methanol production, which is both rare and appealing. At overpotential of 285 mV, copper selenide nanocatalysts electroreduce CO_2 to methanol with a maximum current density of 41.5 $mAcm^{-2}$ and a Faradaic efficiency of 77.6%. In the creation of methanol, copper and selenium in structures function well together. In comparison to prior works, the FE and current density for methanol generation are quite high [30].

2.1.1.6 Cubic Cu_2O on a carbon shell doped with N

Cuprous oxide (Cu_2O) is a promising ethylene catalyst, although its stability and selectivity are lacking. This catalyst was created to generate C_2H_4 via CO_2 electroreduction. Cu_2O cubic nanocrystals spread evenly on the NCS surface by approximately 150 nm width. The Cu_2O/NC shell coated glassy carbon electrode demonstrated great stability and excellent ethylene efficiency (24.7%) at 1.3 V (vs. flexible hydrogen electrode). Because of the broad distribution of Cu_2O cubic nanocrystals and the multiple pyridine-N layers in the NCS, Cu_2O/NCS has extraordinary activity [31].

2.1.1.7 Properties of Surfaces of copper single crystals

The reactivity of C2 products on Cu(111), Cu(100), and Cu(110) single-crystal surfaces explains one important reason for their selectivity by CO_2 reduction. In all single crystal surfaces, the Cu(100) catalyst required the least amount of overpotential for CO_2 to ethylene conversion [31].

2.1.1.8 Properties of Mn

Mn-based heterogeneous catalysts can be efficient and selective electrocatalysts for converting CO_2 to carbon monoxide (CO) by modulating the electronic structure of Mn atoms via halogen and nitrogen dual coordination with a current density of -10 mAcm^{-2} and a low overpotential of 0.49 V, the CO faradaic efficiency (FECO) reaches up to 97%. Furthermore, at overpotential of 0.49 V, the turnover frequency (TOF) for CO_2RR can reach 38347 h^{-1} [39].

2.1.2 Metal Oxides

Metal oxides are naturally occurring chemicals that are highly catalytic. Many oxides of various metals, such as Zn, Cu, Sn, Fe, Ag, and others, exist abundantly in nature or can be treated in the laboratory.

2.1.2.1 Cu_2O and its ZnO composite for the reduction of CO_2

On the stainless-steel surface electrodeposited with Cu_2O film display against the anodized copper electrode, a higher CO_2 electroreduction rate into CH_3OH was obtained. The improved production of Cu_2O film was attributed to the presence of copper in Cu (I) form, which plays an important role in the selectivity of methanol from CO_2. After 30 minutes of continual reaction, the CH_3OH yield began to decrease and methane began to develop as a result of the concomitant reduction of Cu(I) to Cu(0). When using a GDE of (CB = 6: 5 [by weight], CuO/ZnO = 3/7), and a similar amount of H_2, the reduction products were primarily C_2H_5OH with a minor amount of HCOO- and CO. Maximum FE of 16.7% for C_2H_5OH production and maximum selectivity of 88% were found at -1.32 V vs. Ag-AgCl, with a partial current density of 4.23 mAcm^{-2}, which is almost 50 times more than that obtained on a sintered oxide electrode [23].

2.1.2.2. Mesoporous nanosheets of SnO_2

Mesoporous SnO_2 nanosheets that are efficient, resilient, and selective for CO_2 electroreduction have been described. A faradaic efficiency of 87% and a high partial current density of -45mAcm^{-2} were achieved for HCOO- at a tolerable overpotential of 0.88 V, outperforming other GDEs in aqueous media. The C-SnO_2 demonstrated a strong CO_2 reduction rate for the formate, with a maximum combined FE of formate and CO of 80% at 0.8 V vs. RHE [24, 25].

2.1.3 Metal Organic Frameworks

These are made up of a metal atom connected to an organic linker. MOFs have received a lot of interest recently due to their outstanding catalytic activity and applications in a range of industries due to their high conductivity, stability, and variety of structures for each reaction. They can easily absorb carbon dioxide, making them useful for electrocatalytic CO_2 reduction [21]. MOFs are created by combining metal ions (such as Cr, Mn, Fe, Co, Cu, Ni, etc.) and organic ligands, and the resulting compounds have an individual crystal structure, pore size distribution (3.0 - 3.5), high area (500 - 6240 m^2g^{-1}), very low density, and small accessible volumes (0.4 - 3.6 cm3 g-1). Yaghi 142 discovered MOFs in the 1990s, and more than 20000 varieties of MOFs have been synthesized and recognized in a variety of applications to date. A collection of MOFs-based electrocatalysts for CO_2 electroreduction is provided in Table 2.1.

2.1.4 Bi-metallic Catalysts

Bimetallic catalysts are more favorable than monometallic catalysts in practice due to differences in their electrical arrangement, surface composition, oxidation state, and so on. Bimetallic catalysts are typically available in six different structures: crown-jewel structure, hollow structure, hetero-structure, core-shell structure, and alloyed structure.
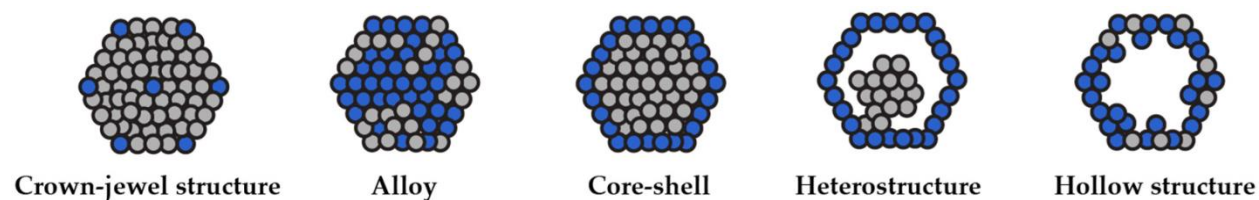
Fig 2.3 Bimetallic nanoparticles with various configurations shown schematically [40]

2.1.5 Factors that have an impact on bi-metallic catalysts

The key parameters that determine the catalytic characteristics of bimetallic catalysts in diverse reactions are discovered to include particle size and shape, structure, composition, surface area, and porosity, among others. The overview of these influences on catalytic characteristics is shown in Figure 2.4 In addition, the consequences of a few other factors are examined in the next section [40].

2.1.5.1 Size and shape of the particles

The surface area of metal particles increases with decreasing size because the total surface area of metal particles is proportional to the square of the diameter of nanoparticles. Because the bulk of chemical reactions occur on the surface of the catalyst, lowering particle size increases catalytic activity.(citation 46,47).Slower reactions are induced by gradually shrinking the size of the nanocatalysts, whereas increasing the size of the catalyst decreases the rate of reaction. In photochemical hydrogen generation utilizing Pt nanocatalysts, there is a critical size of metal particle (typically 3 nm), and any movement above or below will slow down the chemical reaction.(48 citation)

2.1.5.2 Effect of Structure

Bimetallic catalysts with specific properties offer improved versatility in design for activity and selectivity of the catalyst when compared to monometallic catalyst systems. It is widely assumed that the catalytic performance of mono- and bimetallic catalysts is substantially influenced by metal particle size. Other parameters that may influence the catalytic activity of bimetallic catalysts in diverse chemical processes include the kind of support, the metal-support contact, and the structural effect. Intermetallic complexes, cluster-in-cluster formations, and core-shell structures are formed when two metals develop separate destitution modes.

2.1.5.3 Composition effects

Changing the composition has several advantages; it minimizes the poisoning impact and produces a new reaction pathway with specific selectivity. Furthermore, it may produce a synergistic action that changes the electrical arrangement and so boosts catalytic activity. Alloy and bimetallic nanocatalysts can also improve heat stability in some chemical processes [52].

2.1.5.4 Surface area and porosity

It should be noted here that it is difficult to isolate the influence. Surface area differs from surface chemistry. There are two methods for producing high surface areas. The first is to produce small metal particles with a high surface area to volume ratio. The second approach is to create materials with a significant void surface area (pores) in relation to the bulk carrier material. Highly distributed supported metal catalysts and gas phase clusters are pertinent to the first technique

outlined above, whereas microporous materials such as amorphous silica, zeolites, inorganic oxides, and porous carbons are applicable to the second. There is a strong relationship between surface area, pore size, and pore volume; that is, if the pore volume is large, the surface area is large, and if the pore size is small, the surface area is large. Porosity creation can result in a larger surface area than particle size decrease, especially if the pores are small.
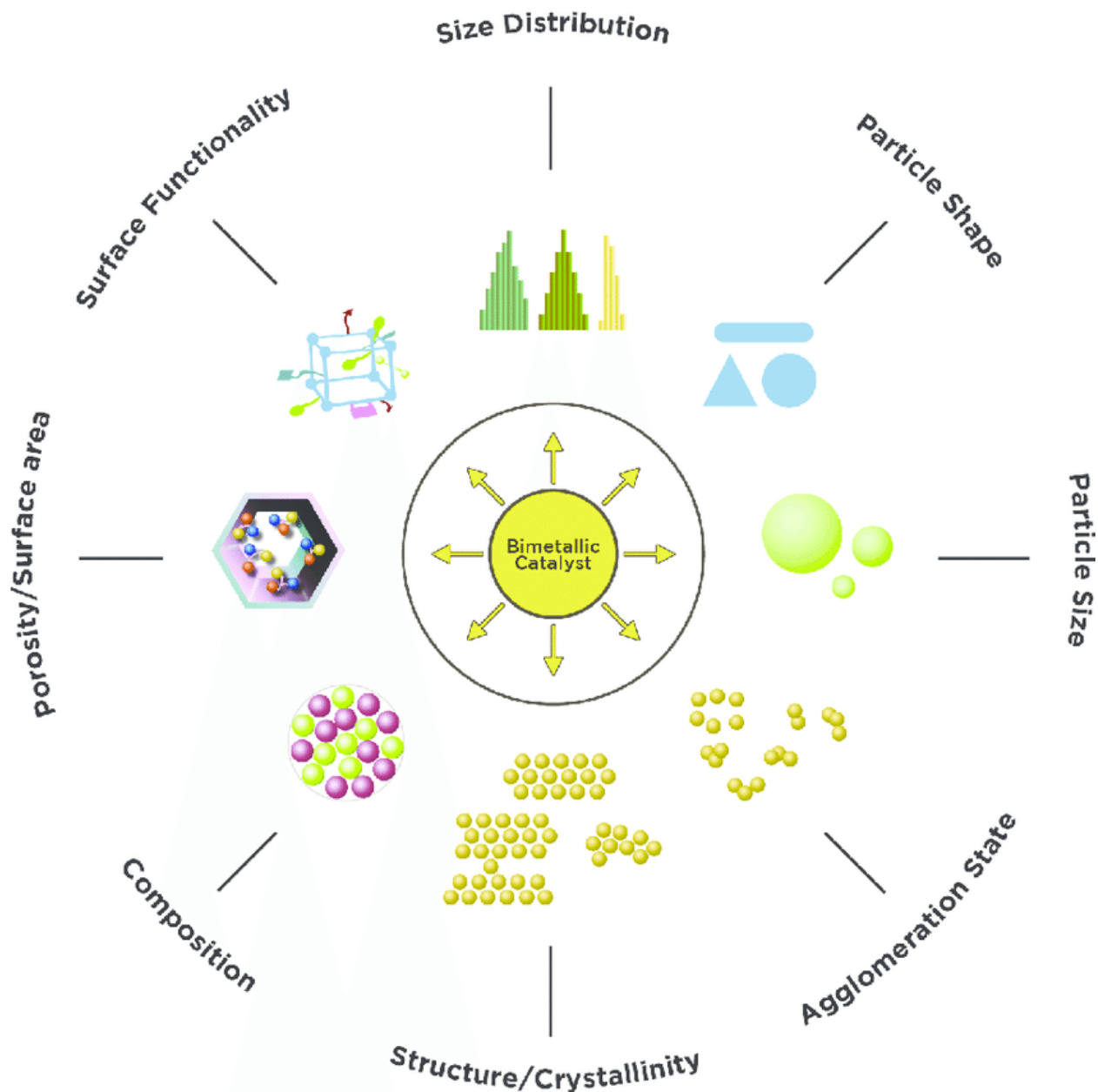
Fig 2.4 variables that determine how well bimetallic catalysts work as catalysts in certain processes [40].

Summary

The basics of electrocatalytic CO_2 reduction are first covered in the chapter on the literature review. Following that, various reaction products—of which methanol is the most significant—as well as various reaction pathways for CO_2 reduction are explored. We carefully examined reaction performance characteristics such Faradaic efficiency, stability, and electrochemical cell design. Examples are used to define various electrolytes and CO_2 reduction kinds. The major subject of Catalyst was covered last. Examples of the performance of previously investigated and tested catalyst materials for electrochemical CO_2 reduction were compared.

Chapter 3

Review on Characterizations Methods and Experimentation

3.1 Synthesis Processes

Numerous techniques have been developed for the correct manufacture of the catalyst material in the lab. Among them, some can be carried out without the use of special tools while others do. The desirable size, appropriate surface qualities, and the type of material involved—such as semiconductors, metals, polymers, ceramics, etc.—are the major factors in determining the catalyst synthesis procedure to produce the necessary NPs. These techniques have been investigated and refined in order to boost our catalyst's yield and provide superior structural and pure results. Some of these techniques are covered below.

3.1.1 Solvothermal Synthesis

It is a method used to create a variety of materials, including ceramics, metals, polymers, and semiconductors. Precursor interaction during synthesis is aided by the use of a solvent at moderate to high pressure (usually between 1 atm and 10,000 atm) and temperature (between 100°C and 1000°C). The procedure is referred to as the "hydrothermal process" if water is the solvent employed. The supercritical water temperature (374°C) is frequently maintained for the hydrothermal synthesis process. A wide range of geometries, including thin films, single crystals, bulk powders, and nanocrystals, can be created with this technique. Additionally, the management of chemical of interest concentration organizes the formation of crystals (rod (2D), sphere (3D), and wire (1D) shapes. It can be utilized to create unique, thermodynamically stable structures that are sluggish and difficult to create using other synthetic pathways. Since 80% of the literature in

the last decade concentrated on nanocrystals, this review will highlight some recent developments including the solvothermal method and nanocrystalline [41].
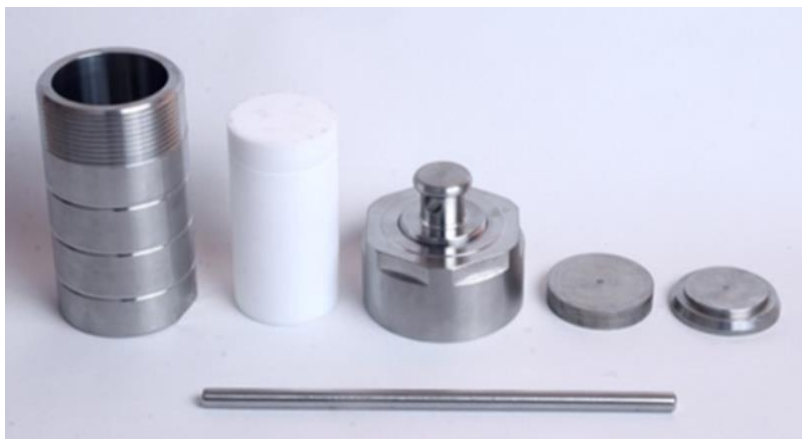
Fig 3.1 For the hydrothermal reactions, an autoclave [42]

3.1.1.1 Synthesis of CuO/Cu-MOF

Typically, 40 mL of DMF were stirred magnetically at room temperature while 2.0 mmol of 1,4-BDC (0.332 g) and 0.65 mmol of $Cu(NO_3)_2 3H_2 O$ (0.175 g) were dissolved in a certain order. The aforesaid mixture was then stirred continuously for 30 minutes while receiving dropwise additions of 4.0 mL of KOH (0.4 mol/L). In an autoclave, the solution was transferred and heated to 100.0 °C for eight hours. To create the finished product, the acquired blue precipitate was repeatedly washed with DMF and then with ethanol before being dried at 60.0 °C in a vacuum oven overnight. The steps for creating bare CuO and Cu-MOF are the identical as those described above, with the exception that KOH and 1,4-benzenedicarboxylate (1,4-BDC) were not used, respectively [53].

3.1.1.2 Synthesis of Mn:Cu@MOF

We modified the prior synthesis technique and used it. Typically, in 40.0 mL of DMF with a magnetic stirrer at room temperature, 2.0 mmol of 1,4 BDC (0.332 g), 0.65 mmol of $Cu(NO_3)_2.3H_2O$ (0.157 g), and 0.65 mmol of $Mn(NO_3)_2.4H_2O$(0.157 g) were dissolved in succession with various ratios of Manganese and copper. The aforesaid mixture was then gradually supplemented with 4.0 mL of KOH (0.4 mol/L) while being continuously stirred for 30 minutes. The mixture was moved into an autoclave and heated to 100.0 °C for 8 hours. In order to create

the finished goods, the acquired blue and light blue precipitates were repeatedly washed with DMF and then ethanol, respectively [53].

3.2 Characterization Methods

3.2.1 X-ray Diffraction

It offers details on the shape, components, and crystallite size of the material and is one of the most significant and popular methods for material characterization. It employs X-ray radiations that strike the substance at an angle from the source and pass through it. The intensity is measured and the diffraction angle is computed. The number of radiations that a material deflects from a particular plane at an angle reveals details about the structure and morphology of the material. The double particle/wave character of X-rays is used to gather information on the configuration of crystalline materials during X-ray diffraction (XRD). The main applications of the technique are material identification and characterization based on their X-ray form. The first thing that happens when a monochromatic X-ray incident beam interacts with an object material is that the target substance's atoms scatter the incident X-rays, as depicted in Figure 3.2. Diffraction is the term for the destructive and constructive interference that the dispersed X-rays cause in solids with correct structure. The directions of expected diffractions are determined by the size and form of the material unit cell. The diffracted wave intensities depend on how the atoms are arranged in the crystal structure. Many substances don't contain a single crystal; instead, they are made up of numerous tiny crystallites oriented in all conceivable directions. This is known as polycrystalline powder or aggregate. The X-ray beam will see all accessible interatomic planes when an object with randomly focused crystallites is exposed to it. All the material's diffraction peaks will be detected if the experimental angle is scientifically changed [44].
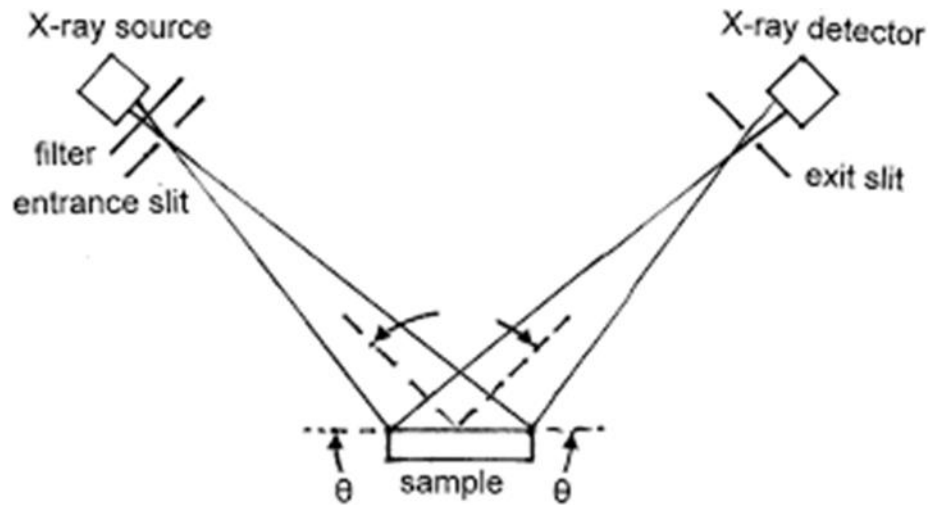
Fig 3.2 Schematic Illustration of the XRD Process [42]

3.2.2 Scanning Electron Microscopy (SEM)

A high-energy electron focused ray is utilized by the scanning electron microscope (SEM) to produce a variety of signals at the specimen's solid surface. According to Figure 3.3, the high-energy electrons pass through the material and exit through the other end. The signals of the interactions between the electron beam and the sample will disclose information about the substance, such as its chemical composition, crystalline structure, exterior morphology (texture), and materials orientation. In a variety of applications, spatial variations in these attributes are seen in a 2-dimensional picture, and data are gathered over a selected region of the sample surface. The areas that range in size from roughly 1 cm to 5 microns in breadth can be distinguished using the scanning approach by straightforward SEM procedures (magnification varied from 20X to about 30,000X, 3-D resolution of 50 to 100 nm). This technique is only useful for semi-quantitatively or qualitatively determining crystalline structure, crystal orientations, and chemical contents (by employing EBSD and EDS, respectively). The SEM is skilled at performing analyses of a particular region or set of points on the sample object. The EPMA and this gadget have a lot in common in terms of function and design, and they still have a lot in common in terms of capabilities [45].
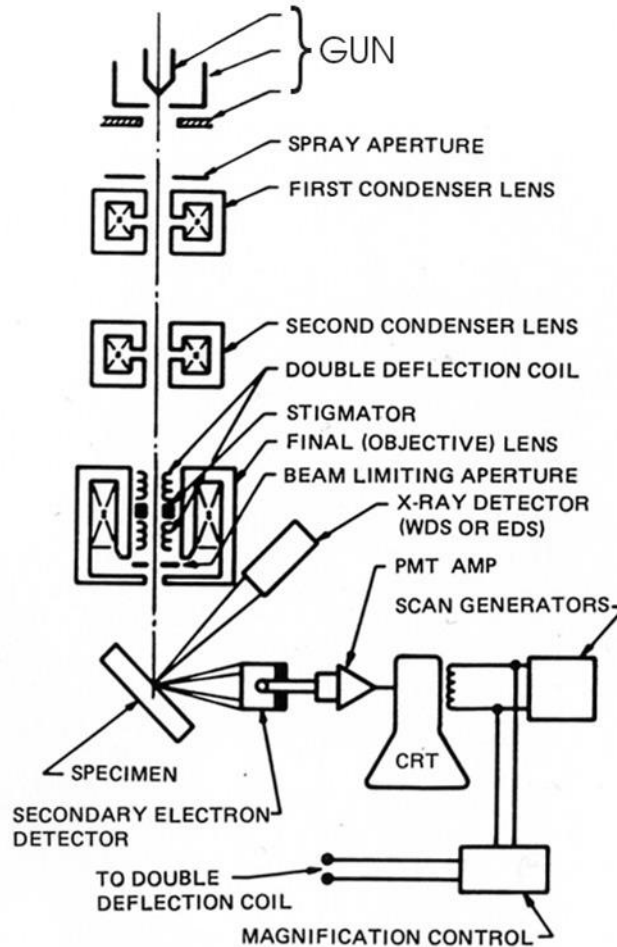
Fig 3.3 Schematic Illustration of the combined SEM-EPMA's electron and x-ray optics [45]

3.2.3 Energy Dispersive spectroscopy (EDS)

The amount of distinct elements found in a nanoparticle can be determined using the elemental analysis technique known as EDS. This method provides the number of substances at a certain location but not the total amount of each element. To obtain a nanoscale image of the particles through them, it is typically paired with SEM or TEM, and EDS analyzes that nanostructure. Early in the 1970s, EDS became a single commercial product and quickly overtook WDS in popularity. Because the EDS doesn't have any moving parts like the rotation detector in WDS, its overall structure is fairly straightforward. As shown in Figure 3.4, the EDS systems are reasonably quick since the sensor collects the X-ray energy signal from all series elements in a sample at roughly the same time rather than gathering signals from individual X-ray wavelengths. Around 150–200 eV is the typical energy dispersion resolution, which is less than WDS resolve. O (Z=8) rather than

C (Z=6) is the lightest component that can be located. However, key advantages like low cost and quick analysis render these drawbacks inconsequential [44].

3.2.3.1 Energy Dispersive Spectra

A graph between X-ray energy and power is known as the EDS band. Because both M or L lines of heavy elements and K lines of light elements are visible in this array, both light and heavy elements can be seen in a range of spectrum from 0.1 to 10-20 keV.
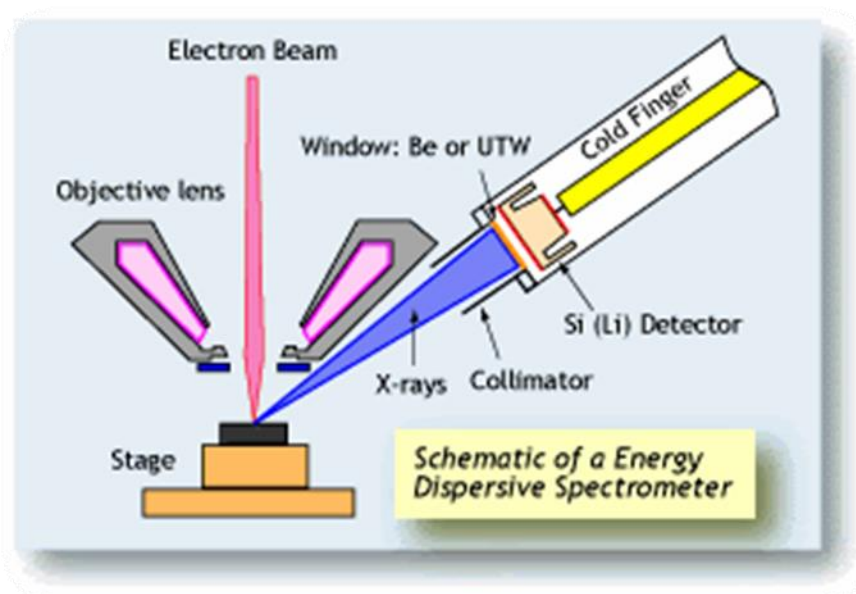
Fig 3.4 Schematic Illustration of EDS [44]

3.2.4 Thermo gravimetric Analysis (TGA)

Weight losses in a substance with a change in temperature (or time) around an ordered environment are calculated using thermogravimetric analysis (TGA). The determination of thermal stability, volatile content, moisture, organic linker in a sample, and the components percent composition of a compound are the main applications of this characterisation approach. Figure 3.5 displays the instrument diagram with output [46].

3.2.4.1 Applications

• Low molecular weight polymers with residual solvent content

- Temperature of decomposition

- Oxidative stability

- The moisture content of inorganic and organic components

- Plasticizer content of polymers

- Residual solvent content

- Carbon black content

3.2.4.2 Operational principles

The basic idea is that a certain gas environment, such as Ar, air, or another gas, is used to gradually raise the temperature from zero to the desired ultimate temperature. Now, as the temperature rises, the sample's contents begin to evaporate. Typically, moisture is the first component to be removed from a sample, changing the sample's mass. Throughout the operation, this mass is regularly monitored on the weight balance that is situated outside the furnace. Other volatile substances, such as organic residue, begin to leak after dampness. The primary point on the curve represents the temperature at which a material begins to breakdown, which is known as the material stability. After then, the line abruptly declines, significantly reducing the amount of material. The stability of the material is decided by this temperature, which is known as the decomposition temperature. The final mass residue is recorded at the end of the procedure, and the overall mass loss is computed.
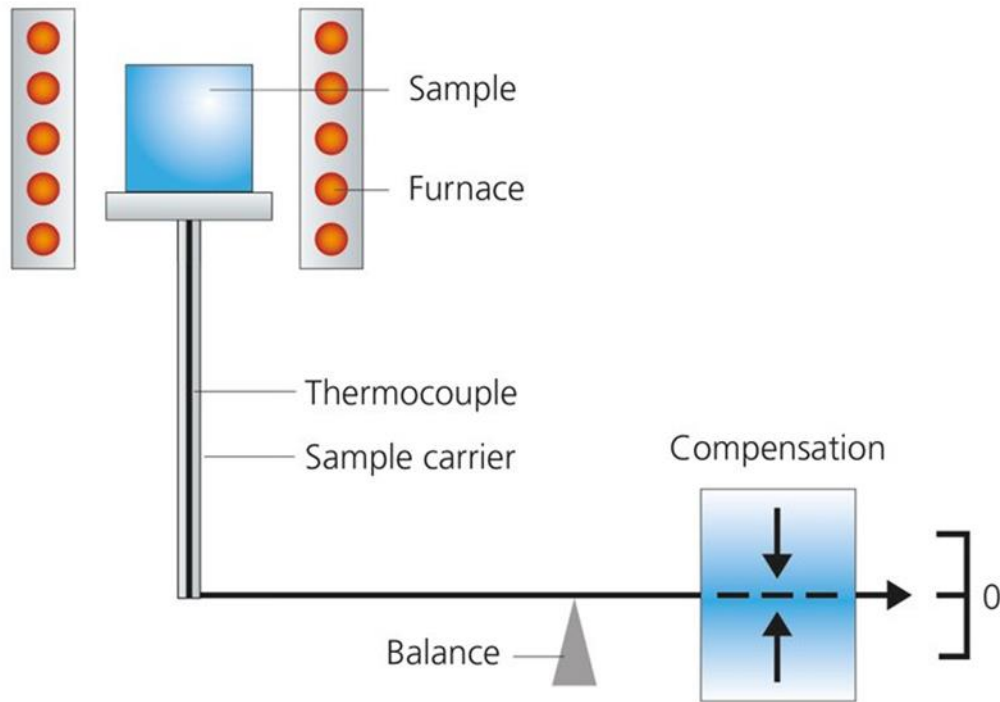
Fig 3.5 Schematic Illustration of the whole TGA System and Instrument [46]

3.2.5 BET Analysis

This characterization method, which involves adsorption and desorption, is used to calculate the material's specific surface area, pore volume, and pore size. By utilizing Langmuir pore size distribution equations, it is also utilized to quantify the pore size distribution in a sample.

Fig 3.6 Schematic Illustration of BET Equipment [46]

3.2.5.1 Measuring and instrumental principle of BET

The BET instrument BET Nova 2200e (Quantachrome, USA) defines the pharmaceutical sample's specific surface area (m²/g). Nitrogen is used for drying samples at high temperatures in a vacuum. Except if instructed we use standard measurement points of P/Po of 0.1, 0.2, and 0.3. The volume of adsorbed gas to the surface of the particles is measured at the boiling point of nitrogen (-196°C). The amount of attached gas is correlated to the overall particle's surface area including surface pores. The specific surface area and the absorbed gas are measured using the BET theory. Most frequently, nitrogen gas that has been adsorbed on the surface is employed. Adsorption of gas also makes it possible to measure the size and volume distribution of micropores (0.35–2.0 nm). A schematic illustration of the BET instrument is shown in Figure 3.7.
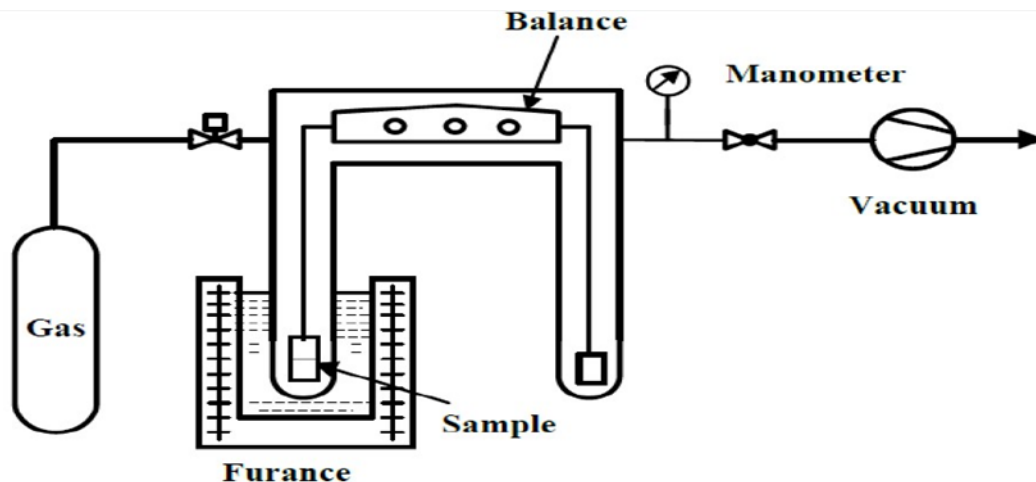
Fig 3.7 Schematic Illustration of the BET procedure [44]

3.2.6 Fourier Transform Infrared Radiations (FTIR)

The preferred approach to infrared spectroscopy is FTIR. When two IR rays contact, some of them pass through the substance while others are absorbed by it. The next indication at the indicator is a band that shows the material's molecular "fingerprint." The primary benefit of infrared spectroscopy is that different chemical structures produce diverse spectral fingerprints.

3.2.6.1 Principle of operation for FTIR

The Michelson interferometer is the primary component of the FTIR setup, as shown in Figure 3.8. The interferometer receives infrared radiation from the source. One beam-splitter, two mirrors, and an interferometer are its main components. The beam splitter reflects half of the rays' (IR) energy while transmitting the other half. Two split beams collide with an oscillating mirror and a fixed mirror. The dynamic mirror's primary job is to change the optical lengths of the path to cause light interference between the two beams. By removing the dynamic mirror from the splitter, a path difference () will be introduced. The changing of route difference and the crystallographic plane diffraction are nearly comparable (Figure 3.8) [47]. Intermittently, the two divided beams will exhibit constructive and destructive interference, with continual changes in the value.
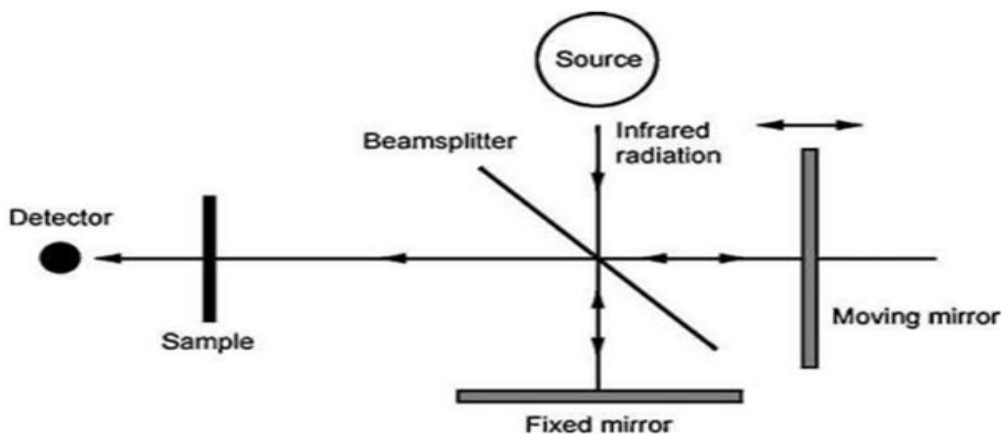
Fig 3.8 Schematic Illustration of FTIR [47]

3.3 Electrochemical Testing

3.3.1 Formation of ink

The catalyst ink is always created to deposit the catalyst onto the surface of the glassy carbon electrode for every electrochemical reaction that takes place there. Depending on the type of catalyst and its solubility, several methods and ratios are used to create ink. While Nafion serves as a binding agent, water and ethanol are used as aqueous solvents for homogenization. Before use, the ingredients are combined in the needed quantity in a tiny vial and ultrasonically processed for around 6 to 8 hours. With a pipette, ink is typically dropped drop by drop onto the electrode surface before being used.

3.3.2 Electrolyte

An aqueous liquid called the electrolyte transports ions from one compartment to another. Depending on the type of catalyst, the configuration of the cell, and the reaction, the electrolyte can be either aqueous, non-aqueous, or solid. Aqueous electrolytes are typically employed in CO_2 reduction processes. In the electroreduction of CO_2, the electrolytes serve as a conduit for the transport of protons and electrons. Catalyst activity and selectivity are influenced by the type and concentration of electrolytes. Electrolytes' minute impurities have the potential to impair catalyst performance by deactivating catalytic sites. When cations are present close to the electrode, they

can affect the relative concentration of charged species, which can affect product selectivity and current density. When the surface charge of the electrolyte cations has the following shape: Na^+, Mg^{+2}, Ca^{+2}, Ba^{+2}, Al^{+3}, and Zr^{+4} increased the rate of electroreduction of CO_2 to CH_3OH. Cation affected the way products were selected. Large cations create CO on an Ag electrode and C_2H4, HCOOH on a Cu electrode when they interact with the Hg electrode. Large cations largely prevented H_2 development. The most popular electrolyte for copper-based catalysts is potassium bicarbonate, or $KHCO_3$, which has a pH of 6.8 when CO_2 is concentrated. High selectivity methanol production is possible with this electrolyte [48].

3.3.3 Electrochemical Cell Design

A piece of apparatus for testing electrocatalytic reactions is an electrochemical cell. An electrochemical cell typically consists of two electrodes, cathode and anode, like an electrolytic cell. These electrodes are located in the two compartments, which also have an aqueous electrolyte, a membrane, and the electrodes. The transport of electrons takes place via the external circuit. Since Hori originally discovered the CO_2 reduction mechanism, several cells have been created. PEM flow cells, H-type cells, microfluidic flow cells, DEMS cells, and solid oxide electrolysis cells are the principal cells among them. A typical electrochemical H-cell is shown in Figure 3.9 [49].

3.3.4 H-Type Cell

Due to its straightforward construction, an electrochemical H-cell is the most well-liked and often used lab-level vessel in contemporary literature. An H-cell typically has two compartments. The counter electrode is housed in the other compartment, while the working and reference electrodes are in the first. The cathode electrode may be a glass carbon electrode coated with ink or a bulk catalyst, such as copper foil. Typically, platinum wire serves as the counter electrode and Ag/AgCl as the reference electrode. The kinetics, mechanism, and most crucially the kind of catalyst that is employed determine the type of electrolyte that is used. The transport of ions takes place through a glass fritz or an ion exchange membrane. The membrane helps transfer ions between the compartments and also stops the produced products from oxidizing once more. A schematic of a basic H-type cell and its components is shown in Figure 3.10. In order to ensure that no oxygen is left in the cathodic compartment during the process, inert gas, such as Ar or N_2, is first purged into

the reactor along with electrolyte to eliminate air from within. After stabilizing the curve to a straight line, a bare run is conducted to see whether there are any impurities. Electrochemical Impedance Spectroscopy is also used to gauge the electrolyte resistance. To concentrate the electrolyte before starting the reaction, CO_2 is first purged through the electrolyte for 30 minutes. Through a regulator fastened to the gas cylinder or a more accurate flow meter, the gas inlet flow rate is measured. A current density vs. potential graph is produced after performing cyclic voltammetry to measure the response of current with applied potential. While CO_2 is being reduced during the reaction, the gas continues to adsorb on the catalyst surface at active sites [49].

Fig 3.9 Schematic Illustration of an active H-type cell

3.4 Methods for electrochemical workstations

The catalyst ink is created, and then it undergoes electrochemical testing. The following electrochemical procedures were carried out on an electrochemical workstation for the electrocatalytic reduction of CO_2:
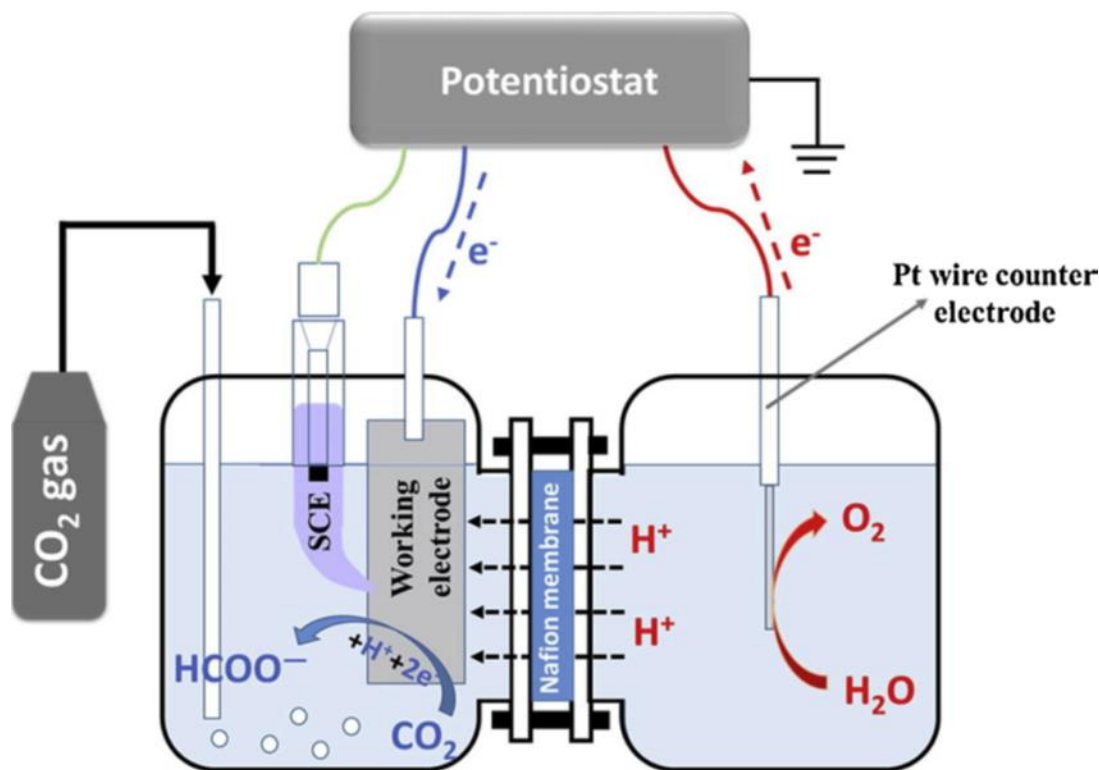
Fig 3.10 Schematic Illustration of H-type Electrochemical Cell [49]

3.4.1 Cyclic Voltammetry

A fantastic and widely used electrochemistry technique called cyclic voltammetry (CV) is used to investigate how molecules oxidize and reduce. It is useful to look at chemical reactions that are catalyzed by electron transfer. This electrochemical method entails operating the workstation via a full cycle. The software that applies the potential range across the two electrodes received the potential range as an input. For each run, sensitivity, sample interval, and scan rate were provided along with a number of segments. One cycle is made up of two segments. The cyclic voltammetry provides information about how the current changes with voltage. During CV, current flows through an external circuit, causing electrons to begin moving from the anode to the cathode. The signal of the current depends on how many electrons result in reduction. The electrochemical cell, which has two compartments, is used to perform CV. To get rid of any oxygen in the cathode compartment, the cell is first purged with Ar inert gas. Following that, CV is carried out and CO_2 is evacuated. The glassy carbon electrode has a catalyst coating on it. When testing the stability of materials, CV is occasionally used to complete lengthy stretches in a single run [50].

3.4.2 Linear Sweep Voltammetry

This approach is used to measure cell current versus applied potential, as shown in Figure 3.11. The potential changes linearly and terminates at a point. This technique is quite similar to the CV except that it only includes one segment, the reduction phase. The CO_2 is adsorbed and reduced at the cathode, and the current density signal indicates the number of electrons responsible for the CO_2 reduction.
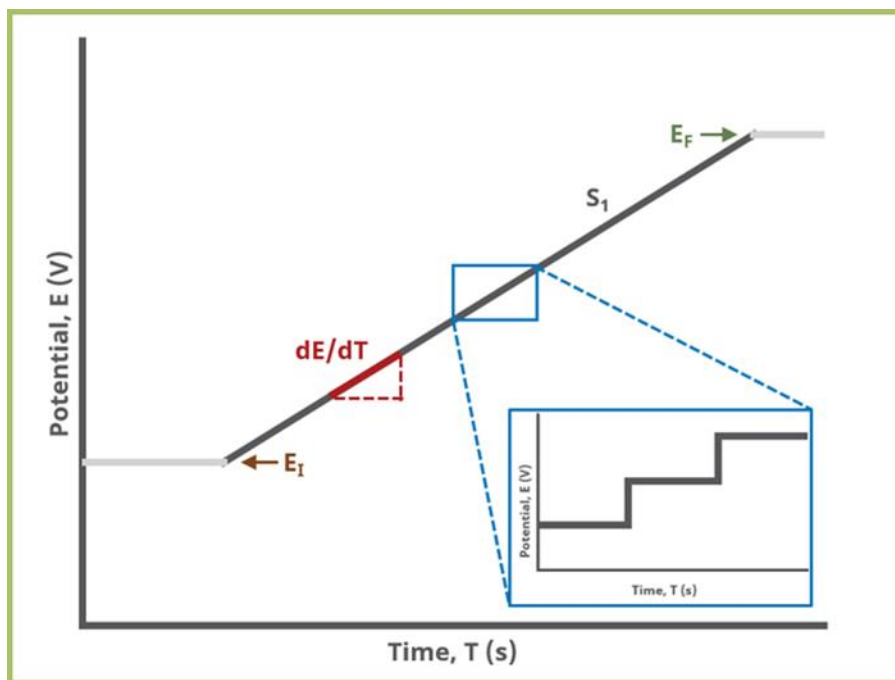
Fig 3.11 Waveform Field Diagram for Linear Sweep Voltammetry (LSV). [48]

3.4.3 Bulk electrolysis

CPE is an electrochemical technique that is used to run lengthy reactions on the surface of catalysts at a constant voltage. The current-time curve is obtained, which provides information on the changing current density over time. If the current density remains stable throughout time, it suggests that CO_2 is being reduced at a constant rate to the desired product. As shown in Figure 3.12, CPE gives a notion of what potential maximum product can be generated. The regulated Potential Electrolysis principle is straightforward. The number of electrons passed per molecule in a given time gives the integrated current and the number of moles of the species' molecules.

43

Faraday's law evaluates (N) the charge that passes through in the given period of the CPE experiment:

$Q = nFN$

where $F = 96500$ C mol$^-$ (Faraday's constant).
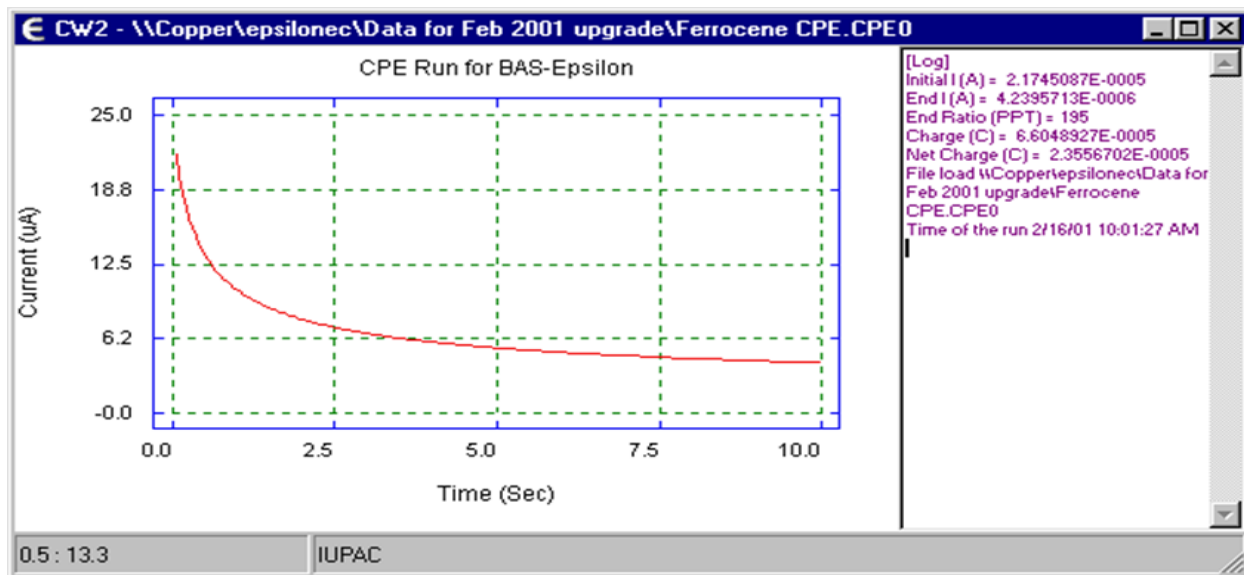
Fig 3.12 Plot of current vs. time for electrolysis at constant voltage [51]

3.4.4 Electrochemical impedance spectroscopy (EIS)

This electrochemical workstation technique allows us to measure the resistance of our system. This comprises electrolyte resistance, ohmic loss, and/or activation losses. Electrical resistance is a measurement of a circuit's ability to resist the flow of electrical current. Figure 3.13 depicts the EIS graph.

According to Ohm's law,

Resistance (R) is defined as the ratio of voltage (E) to current (I).

This well-known law is only applicable to one circuit component, the ideal resistor. A perfect resistor has several properties:

• Ohm's Law is observed at all voltages and currents, and resistance is not frequency dependent.

44
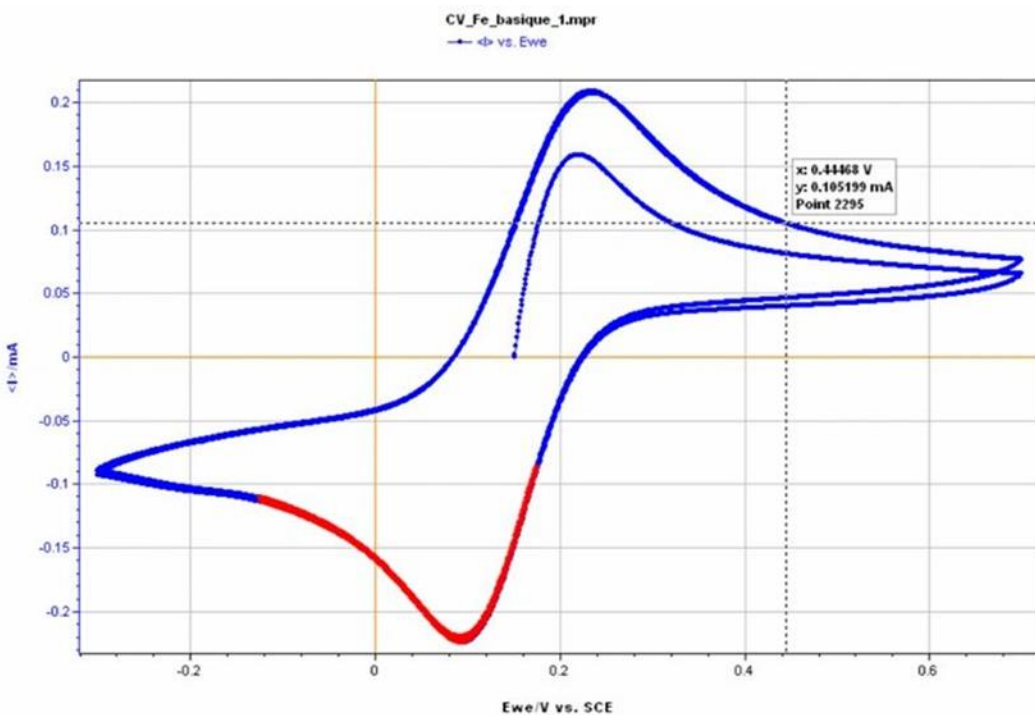
Fig 3.13 the graph of electrochemical impedance spectroscopy [51]

3.5 Techniques for Product Analysis

Following CO_2 reduction in the electrochemical cell, the product gases and liquids must be investigated and subjected to some qualification and quantification processes in order to identify them and assess the faradaic efficiency of our intended products. Among these techniques are:

3.5.1 Gas Chromatography

The gas chromatography (GC) technique is used to determine the gas in a gas mixture. It provides quantitative as well as qualitative analysis. Gas chromatography, more precisely liquid-gas chromatography, involves vaporizing a material and injecting it onto the dome of a chromatographic column. The flow of gaseous, inert, and mobile phases transports the sample through the column. A liquid stationary phase is adsorbed on an inert solid surface in the column. Different gases, such as CO, CO_2, methane, and hydrogen, can be identified using GC. Figure 3.14 shows a representation of GC. The standard was used to calculate the number of distinct gases based on retention duration '[50].

45

Gas Chromatography
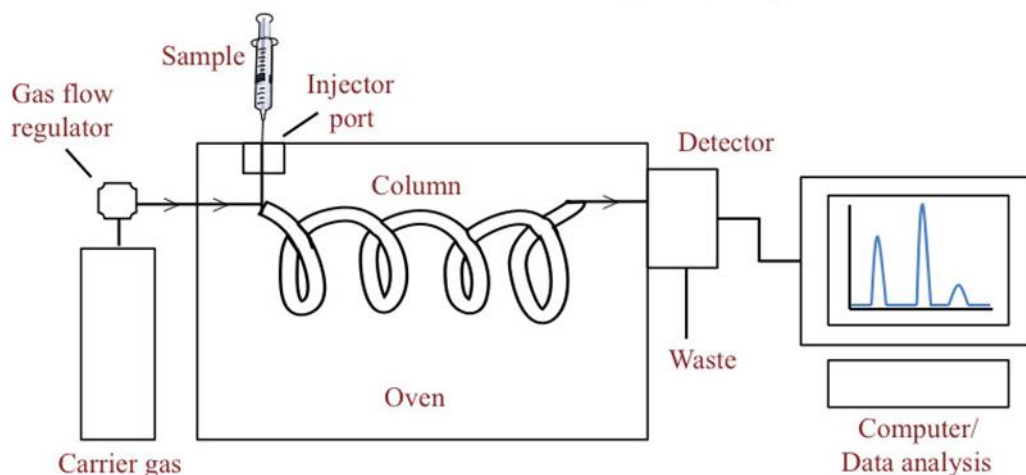
Fig 3.14 Schematic Illustration of GC [50]

3.6 factors for reaction performance

3.6.1 Turnover frequency

At the applied overpotential, it is defined as the total number of electrocatalytic conversions per catalytic site. This is a catalyst performance measure that is used to distinguish between two catalysts based on their frequency. Due to the intricacy of catalyst structure active sites, calculating the exact frequency number of a catalyst can be challenging at times. This phrase is rarely used, however it can be used to determine the inherent activity of a catalyst.

3.6.2 Faradic Efficiency

This phrase is used to quantify the catalyst's ability to generate a product and is defined for a specific product as the ratio of charges passed to that product to the total number of charges passed through the circuit. It is also a measure of the catalyst's selectivity for a specific product. Because the kinetics and energy barrier for CO_2 reduction are typically high, a catalyst with high faradaic efficiency overcomes the necessary energy barrier. For example, Au edge-rich nanowires are one of the most active electrocatalysts in aqueous solutions, with a CO $E_{faradic}$ overpotential of 94% at 0.23 V.

3.6.3 Stability

The stability of a catalyst is an essential aspect in its long-term operation and performance. It is often assessed by performing numerous cycles of cycle voltammetry (CV). Assume a catalyst CV is completed with 1000 cycles. If the current going through the circuit vs. potential graph is consistent and overlaps throughout 1000 cycles, the catalyst is highly stable for electrocatalytic CO_2 reduction. The stability of graphene confined Sn quantum sheets in 0.1 M $NaHCO_3$ electrolyte has been measured to be 18 hours at -1.8V applied potential vs. RHE [52].

Summary

This chapter begins by discussing several chemical synthesis methods such as solvothermal and Hydrothermal processes. Following that, material characterization techniques such as XRD, SEM, EDS, TGA, BET, and FTIR were investigated. The essential principles of these strategies have been documented with diagrams. The entire electrochemical testing process was then discussed, including ink production, electrolyte selection, and H-cell setup. The final section of this chapter includes electrochemical CO_2 reduction workstation analysis methodologies and product analysis techniques such as cyclic voltammetry, linear sweep voltammetry, EIS, and gas chromatography, as well as reaction performance metrics.

Chapter 4   Results and Discussion

4.1 Synthesis and Characterisation

The Mn:Cu@MOFs was synthesized using one pot solvothermal method. The Mn^{2+} and Cu^{2+} of Manganese nitrate and cupric nitrate reacted with OH^- of potassium hydroxide to procreate light blue precipitates of Manganese and Copper hydroxide in DMF solvent, which then aligned with ligand 1-4 BDC at 100°C. The hydroxide of manganese and copper dissolved and partly further exchange into Mn: Cu @MOfs. Different molar rations of Manganese nitrate and copper nitrate are used to prepare three different samples.

XRD Analysis The successful synthesis of Cu-BDC and Mn-BDC has been confirmed through various catalyst characterization studies shown in the fig. 4.1 (a). The structural information and crystal phase were studied by XRD analysis. The main diffraction peaks of Mn-BDC MOF at 23.9°,19.6°,29.2°, 34.1° and Cu-BDC MOF at 10.1°,12.0°,17.5°, 24.7°, which could be absolutely matched to the respective (022),(002),(112), (004), (110),(222), (021), (040) planes and these were the close agreement with previously reported XRD pattern of Mn-BDC and Cu-BDC (CCDC NO. 000410254, 01047327) respectively[66-68].

The spectrum of FTIR showed in the Fig. 4.2 (b) evidently displays asymmetric and symmetric stretching vibrations of COO^- in the region of 1620 and 1391 cm^{-1} respectively. These results clearly shows the de-protonation of acidic COOH after complexation with Mn and Cu ions and can be attributed to carboxyl group (COO^-) matched to the metal center in the acquired MOF .The delicate stretching vibration bands emerging at 1455 and 1607 cm^{-1} which can be allocated to free carboxyl groups. The peak at 1666 cm^{-1} arises from O=C-N (in DMF) deformation mode and vibration of OH^-.The peaks at 756 and 1504 cm^{-1} corresponds to the plane bending vibrations of C=C aromatic ring. In addition, the ring out of plane vibration of 1-4 substituted bond core of linker molecule emerged at 752 cm^{-1} which suggest effective coordination of both metals wit 1-4 BDC [57, 69, 70].

Thermogravimetric Analysis was performed on all the samples of Mn:Cu@MOFs having different ratios shown in the fig. 4.2 (d). Minor weight loss was observed for all MOFs at 170°C which indicate that there was little surface adsorbed moisture. Next weight loss was observed at 225°C

for all samples which we can ascribe the weight loss of coordinated DMF[71]. When temperature increased above 320°C sharp weight loss of almost 40%, 30% and 20% for Mn: Cu(1:2)@MOF, Mn: Cu(1:1)@MOF and Mn: Cu(2:1)@MOF respectively was observed which indicate that organic ligand degradation occurred. further weight losses occurred for all materials and these indicating the residual natural oxides and above 500°C cause the material to decompose into Manganese and copper dioxides[72]. As we can see in the figure when percentage of copper increased no major weight loss occurred for Mn:Cu(1:2)@MOF because it is more thermally stable and shows the strength of bond in the framework. On other hand continuous weight loss observed for Mn:Cu(1:1)@MOF and Mn:Cu(2:1)@MOF because lower thermal stability of manganese.

BET Analysis to examine absorption properties of our best sample Mn: Cu (1:2)@MOF shown in the fig. 4.2 (c). Brunauer-Emmer-Teller (BET) analysis was done in N_2 atmosphere. It was observed that generated isotherm were of type 1 for Mn: Cu (1:2)@MOF which showed that our sample consists of micro-porous structure. The volume of gas adsorbed hikes two time, first at low relative pressure >0.07 and then at high relative pressure value near to 1, which confirms dual structure of our catalyst. Observed surface area of Mn: Cu (1:2)@MOF is 628 m^2g-1 with pore size of 1.6nm and pore volume of 2.24cm^3/g.

Scanning electron microscopy was utilized to examine surface morphology of the MOFs which shown in the fig.1. The images showed the distribution of particles on the surface of MOFs as cluster of irregular shaped 2-D cubic Nano-sheets. Cu-MOF has two dimensional layered structure and manganese has homogeneous laminar structure which is bounded loosely [67]. Bulky particle belongs to Cu and with increasing content of Cu structure show flakes like arrangement while we analyzed the increasing Mn content cause agglomeration between the crystals [64]. EDS analysis was executed to examine chemical constituent and purity of solvothermal Mn:Cu@MOFs. EDS spectrum showed the homogeneous dissemination of Cu, Mn, O, C and K all over the flakes shown in the fig. 4.1.
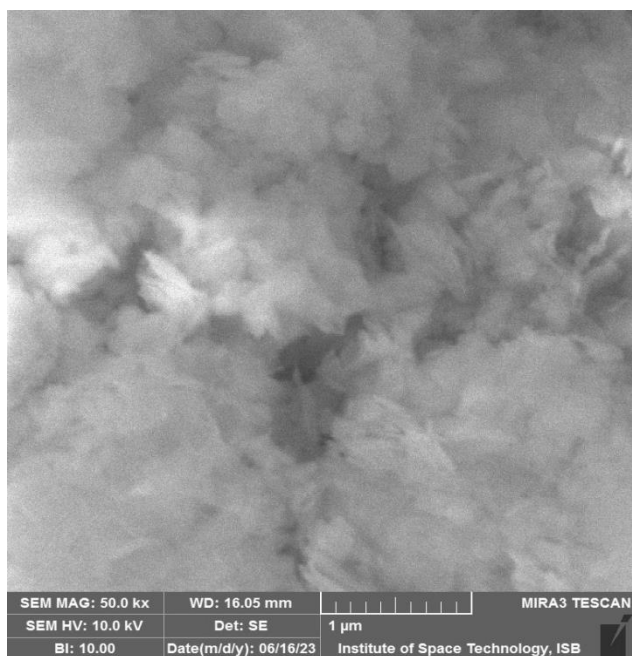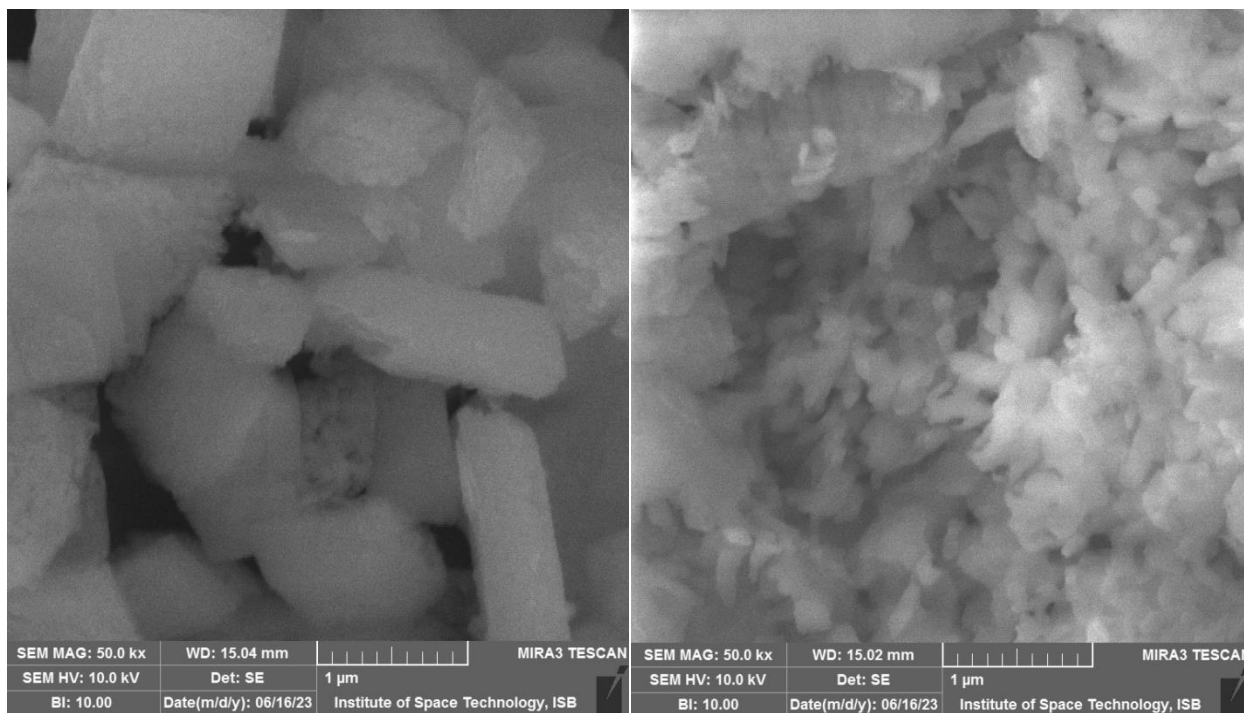
Fig 4.1 SEM images (a) Mn:Cu(1:2)@MOF (b) Mn:Cu(1:1)@MOF (c) Mn:Cu(2:1)@MOF

Table 4.1 EDS analysis of all the materials with atomic and weight percentage

Elements	Weight %					Atomic %				
	C	O	K	Mn	Cu	C	O	K	Mn	Cu
Mn: Cu (1:1)@MOF	42.46	26.29	4.80	13.00	13.45	59.29	28.69	2.12	4.77	5.13
Mn: Cu (1:2)@MOF	32.52	26.30	3.04	15.94	22.20	54.05	31.09	1.82	5.56	7.48
Mn: Cu (2:1)@MOF	38.85	25.95	3.41	19.77	12.02	58.63	26.68	1.9	7.49	5.3
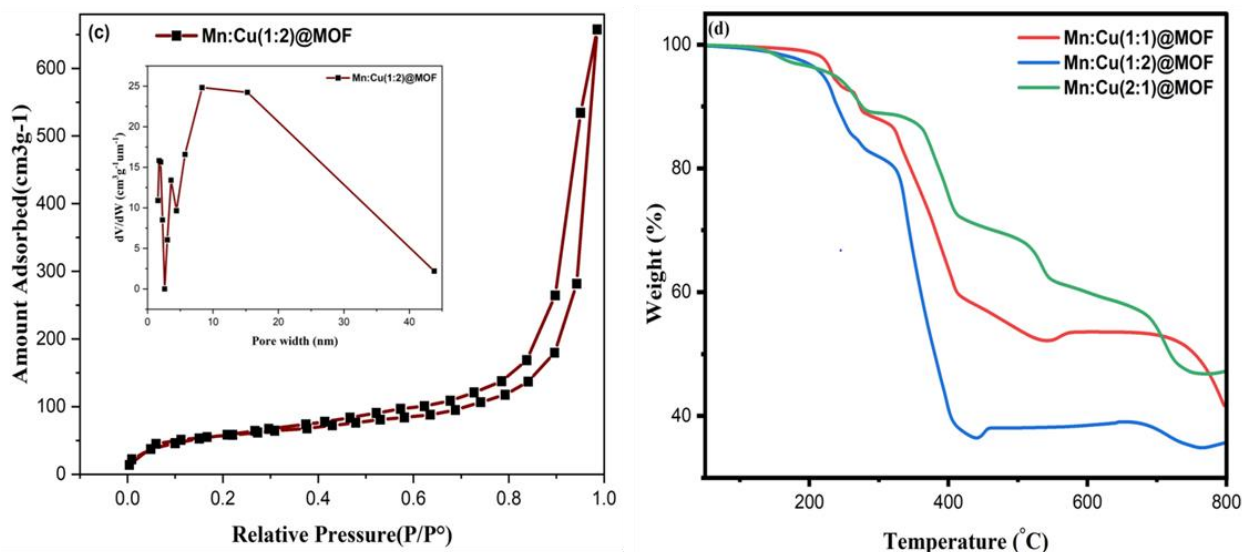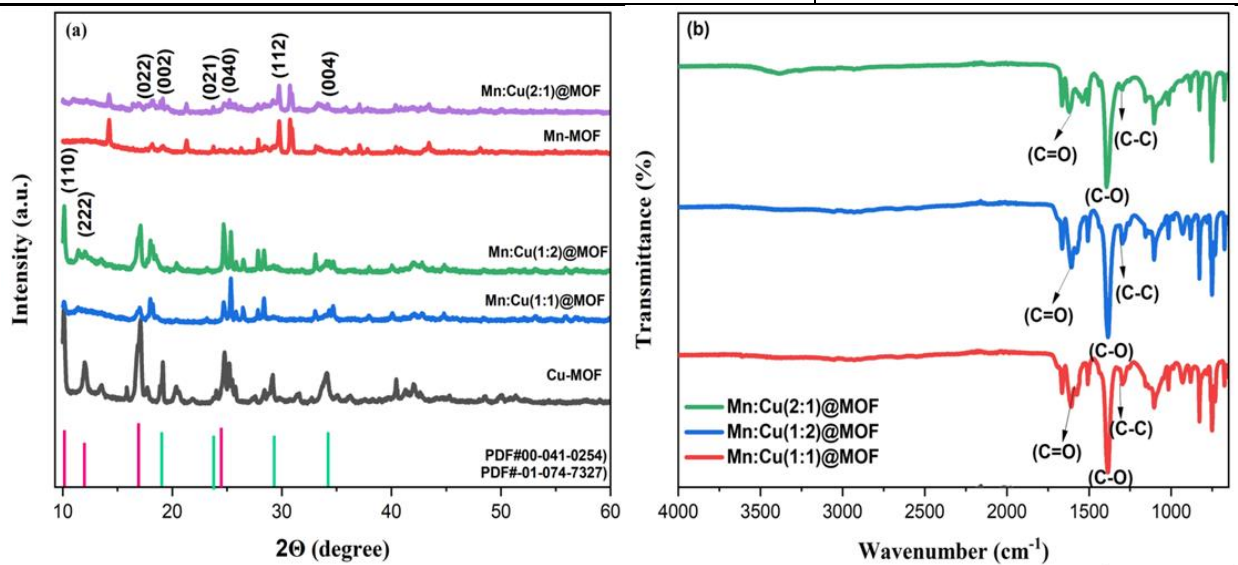
Fig 4.2 (a) XRD spectrum of Cu-MOF, Mn-MOF and Mn:Cu(1:1)@MOF, Mn:Cu(2:1)@MOF, Mn:Cu(1:2)@MOF (b) FTIR transmittance spectrum of Mn:Cu(1:1)@MOF and Mn:Cu(1:2)@MOF, Mn:Cu(2:1)@MOF samples. (c) N_2 adsorption-desorption isotherms with pore size distribution of Mn:Cu(1:2)@MOF (d) TGA curves of Mn:Cu(1:1)@MOF, Mn:Cu(1:2)@MOF and Mn:Cu(2:1)@MOF samples

4.2 Electrochemical performance

The electro-catalytic performance of Cu-MOF, Mn-MOF, Mn:Cu(1:1)@MOF, Mn:Cu(1:2)@MOF and Mn:Cu(2:1)@MOF were tested for Electrochemical CO_2 reduction on a glassy carbon working electrode in 0.1 M $KHCO_3$ aqueous electrolyte. Linear sweep voltammetry was performed for all the samples in the potential range of -2 to -1 vs. (Ag/AgCl) to check the response of current density against applied potential for single Cu-MOF, Mn-MOF and Bi-Metallic Mn:Cu(1:2)@MOF ,Mn:Cu(1:1)@MOF and Mn:Cu(2:1)@MOF as shown in fig.4.3. Among them, Mn:Cu(1:2)@MOF showed the highest current density -58 mAcm^{-2} at -2 V. High cathodic current were achieved in CO_2 atmosphere than in N_2 over voltage regime. Cu-MOF and Mn-MOF showed the current density of -38mAcm^{-2} and -35mAcm^{-2} respectively which is higher than previous reported work[19, 26]. The high current density showed in CO_2 atmosphere assigned to the accessibility of more active sites in Bi-Metallic MOF which increase overall performance as compared to other catalysts. At -2 V Mn:Cu(1:1)@MOF showed high current density of -56 mAcm^{-2} as compared to Mn:Cu(2:1)@MOF value of -51 mAcm-2 as shown in Fig. 4.3 (c, d) The actual reason for this is more copper nodes and active sites available and also have more N contents which promotes proton-electron transfer. Copper helps in proper dispersion due to more adsorption characteristics. As clearly we can see in figures those have more current density which have more copper percentage or equal to manganese. Manganese has less active sites and more resistivity which hinder the promotion of proton electron transfer .As we can see SEM images where agglomeration make the absorption difficult due to lower surface area of manganese which leads to CO_2 conversion difficult.
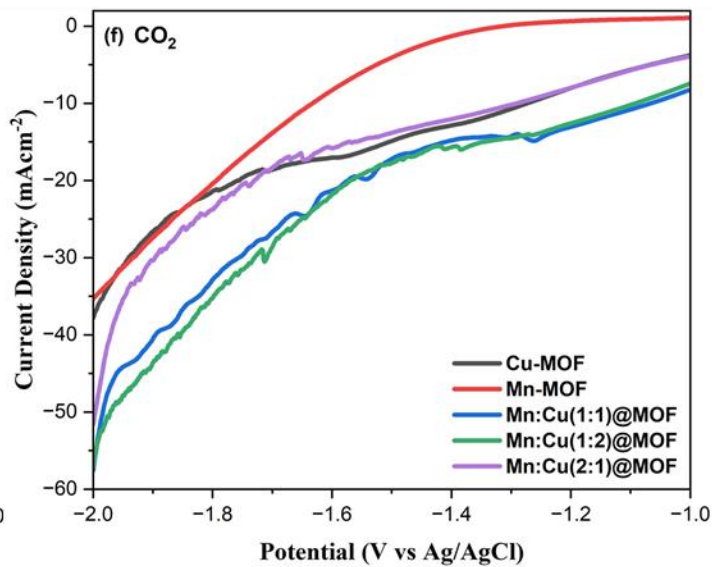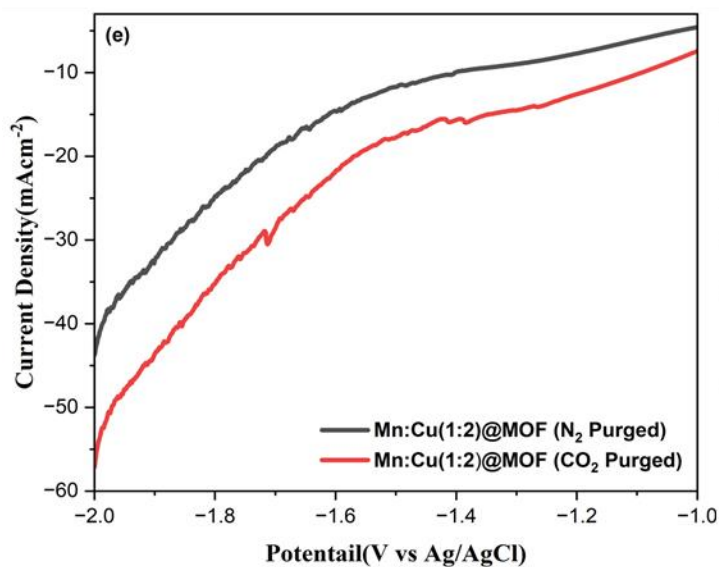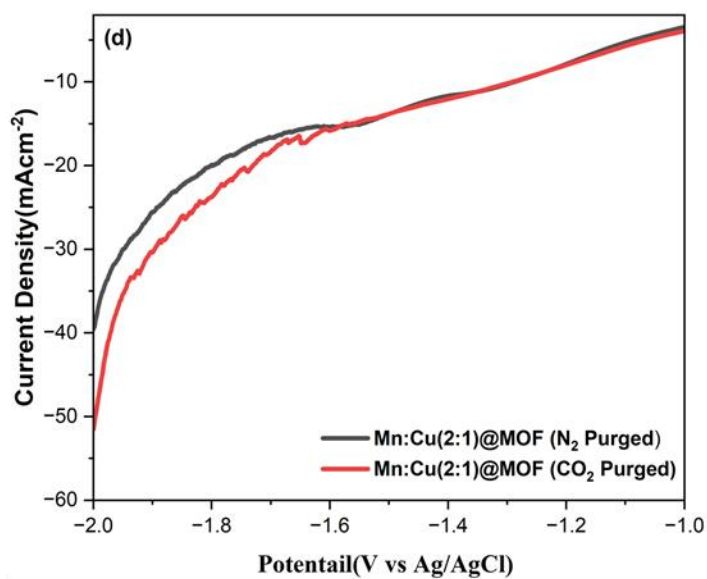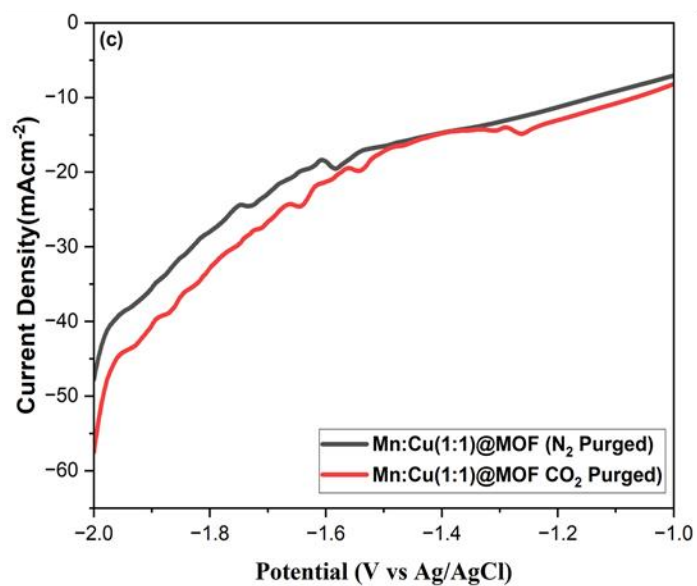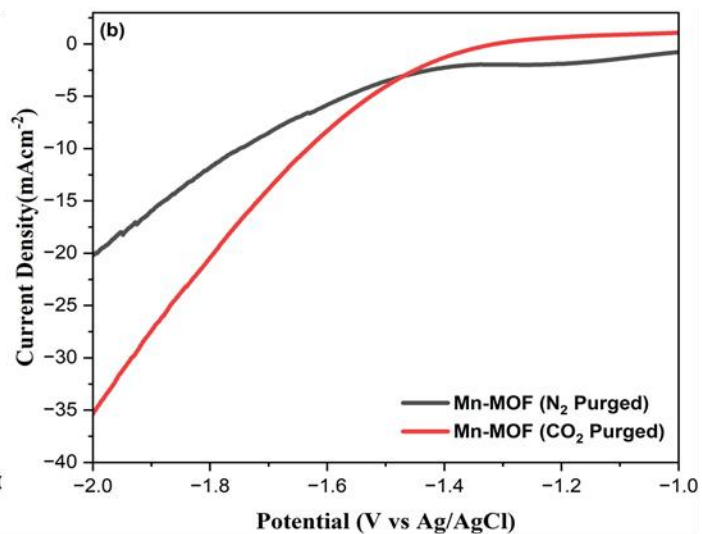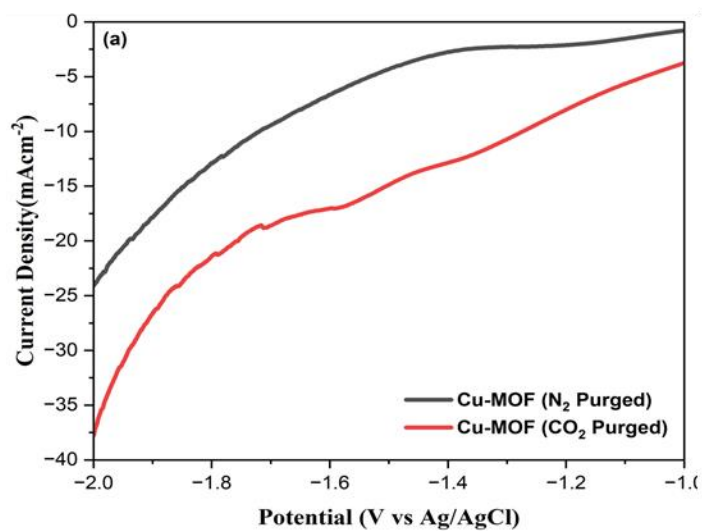
Fig 4.3 LSV comparison of N_2 and CO_2 saturated 0.1 M $KHCO_3$ electrolyte at 10mV/sec scan rate (a) Cu-MOF (b) Mn-MOF (c) Mn:Cu(1:1)@MOF (d) Mn:Cu(2:1)@MOF (e) Mn:Cu(1:2)@MOF (f) LSV comparison of Cu-MOF, Mn-MOF, Mn:Cu(1:1)@MOF, Mn:Cu(1:2)@MOF, Mn:Cu(2:1)@MOF in CO_2 saturated 0.1 M $KHCO_3$ electrolyte.

4.3 Product Analysis

Constant bulk electrolysis was performed in narrow range of voltages from -1.6 V to -1.2 V vs. Ag/AgCl and at the end of each electrolysis process of 20 minutes gas samples were collected through syringe and detected in gas chromatography. Hydrogen, Methane and Carbon monoxide are the only detected end products whose faradic efficiency was calculated. Hydrogen have more faradic efficiency shown in fig.4.4 (a) in case of Mn:Cu(2:1)@MOF as compared to Mn:Cu(1:2)@MOF and Mn:Cu(1:1)@MOF because more percentage of manganese provides less adsorption active sites which leads to take place hydrogen evolution reaction. Due to less surface area and lower conductivity of manganese made the CO_2 reduction reaction difficult. In case of Mn:Cu(1:1)@MOF and Mn:Cu(1:2)@MOF have less hydrogen faradic efficiency due to more active sites of copper and adsorption capacity, hydrogen evolution reaction suppressed and leads to take place CO_2 reduction. CO is the first CO_2 reduction C1 product and percentage of CO is more shown in fig.4.4(c) in case of Mn:Cu(1:2)@MOF at more negative potential of -1.5 V vs. Ag/AgCl this is because of more adsorption capacity of copper and more surface area promotes proton-electron transfer which requires less over potential. CO percentage decrease when potential becomes less negative. In case of Mn:Cu(2:1)@MOF CO percentage is less because binding energy of CO enter at metal surface which poisoned the surface of metal and it could not go on to react further that's why hydrogen evolution reaction more dominant in this scenario. Cu has intermediate CO binding energy which helps to further reduce the CO_2 reduction reaction.

The reduction of CO_2 towards higher hydrocarbons is difficult because of many factors such as hydrogen evolution reaction dominates and CO make the metals poisoned which hinder further reduction. On the other hand activation over potential for proper charge transfer, bubbling effect which creates resistance and lower stability of material make the production of higher hydrocarbons difficult. Methane is important product whose percentage is more in case Mn: Cu (1:2)@MOF shown in fig. 4.4(b) because of more N content in Cu and large surface area. Methane percentage is less at more negative potential and increase when potential reached at -1.4 V vs.

Ag/AgCl which is 54%. As confirmed from literature that at higher negative potential solution has more pH values which hinder further CO_2 conversion. The current density exhibited in the fig. 4.4(d) varies with different cathodic voltages during bulk electrolysis.
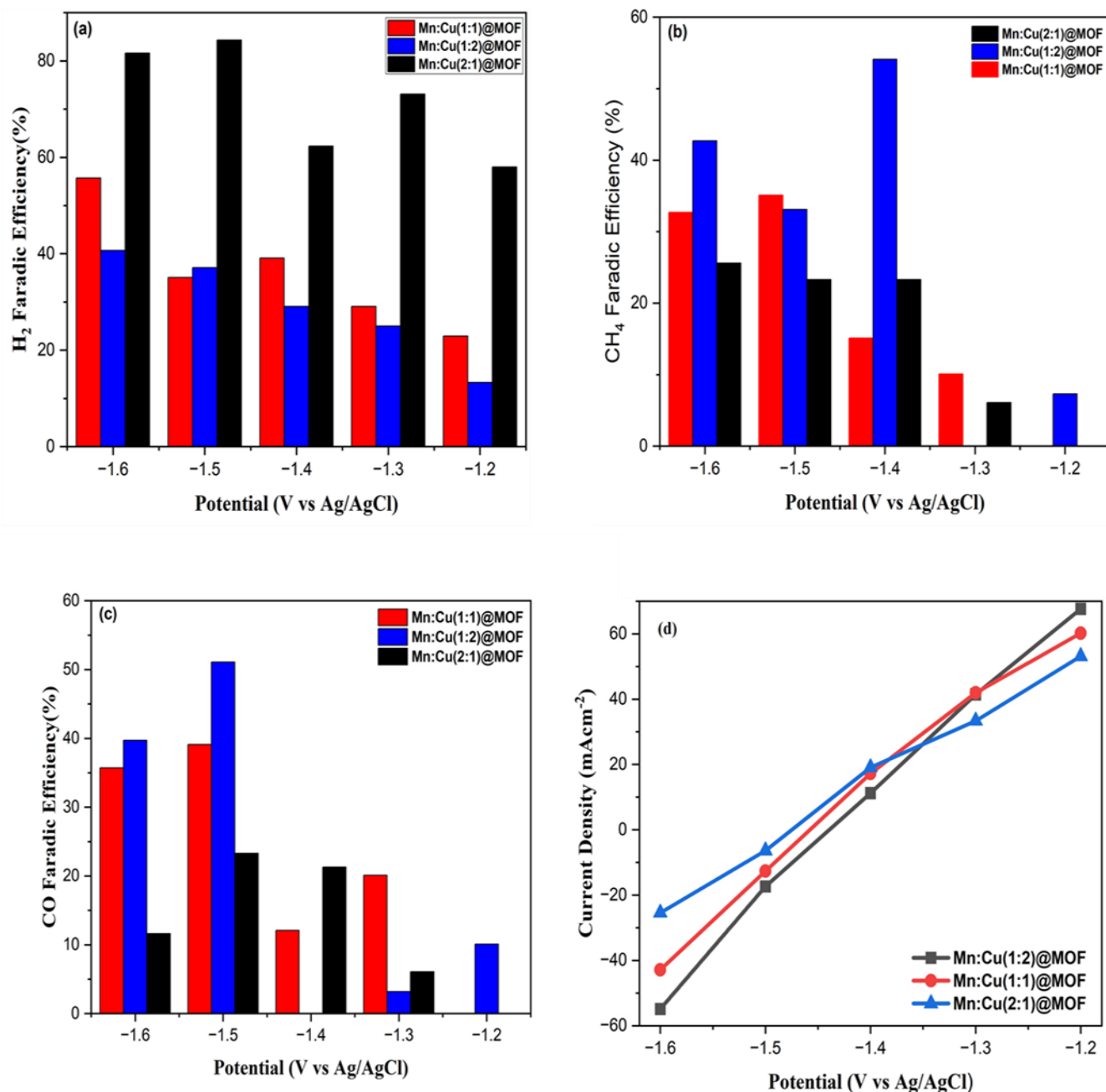

Fig 4.4 CO_2 reduction performance in constant potential electrolysis for Mn:Cu(1:1)@MOF, Mn:Cu(2:1)@MOF, Mn:Cu(1:2)@MOF **(a)** H_2 Faradic efficiency **(b)** CH_4 faradic efficiency **(c)** CO faradic efficiency **(d**) Total current density comparison

4.4 Tafel slope, Stability and EIS performance

Compares Current percentage graphs of catalysts shown in fig.4.5 Mn:Cu(1:2)@MOF, Mn:Cu(1:1)@MOF , Mn:Cu(2:1)@MOF during bulk electrolysis against applied potential at -1.3, -1.4 and -1.5 V vs. Ag/AgCl for 20 minutes. We clearly seen that Mn: Cu (2:1)@MOF current density decreases more as compared to other 2 MOfs, which shows that bubbling effect dominates on the surface of electrode and CO starts to adsorbing on catalysts which results to hydrogen evolution reaction take place gradually and with the passage of time its stability decreasing, At -1.5 V getting stable and then increase variably. Mn:Cu(1:2)@MOF, Mn:Cu(1:1)@MOF are more stable due to more copper percentage as it has large surface area   which created the more active sites on the surface of electrode and this leads to adsorption characteristics.

Conducted the electrochemical Impedance spectroscopy to study electrochemical system. The Nyquist plot revealed that Mn:Cu (1:2)@MOF has smaller charge transfer resistance as compared to Mn:Cu(1:1)@MOF, Mn:Cu(2:1)@MOF, it promotes charge exchange in electrolyte and at high current density yielded hydrocarbons. Mn:Cu(1:2)@MOF have lower over potential which provides linear response and lower impedance. On the other hand Mn:Cu(2:1)@MOF have higher over potential, impedance and lower surface area which hinder the movement of species and results in lower reduction of CO_2 due to lower proton-electron transfer. As depicted in fig. 4.5(e) fitting circuit of all the MOFs which involved the incorporation of resistance, capacitance and Warburg impedance. The calculated error for respective MOFs are as follows 5.4% for Mn:Cu(1:2)@MOF, 5.2% for Mn:Cu(1:1)@MOF and 11.1% for Mn:Cu(2:1)@MOF. The Tafel slope was determined to be 178mVdec^{-1} for Mn:Cu(1:2)@MOF, which is significantly lower than the Tafel slopes of 192mVdec^{-1} for Mn:Cu(1:1)@MOF and 210mVdec^{-1} for Mn:Cu(2:1)@MOF shown in the fig. 4.5(d). The kinetics of electrochemical CO_2 reduction on Mn: Cu (1:2)@MOF exhibit notably faster rate as compared to other two MOFs. The generation of CO species during the sequential hydrogenation process leading to COH and CHO* intermediates and the C-C coupling on the surface of Cu-based catalysts are likely to govern the overall reaction kinetics[34].
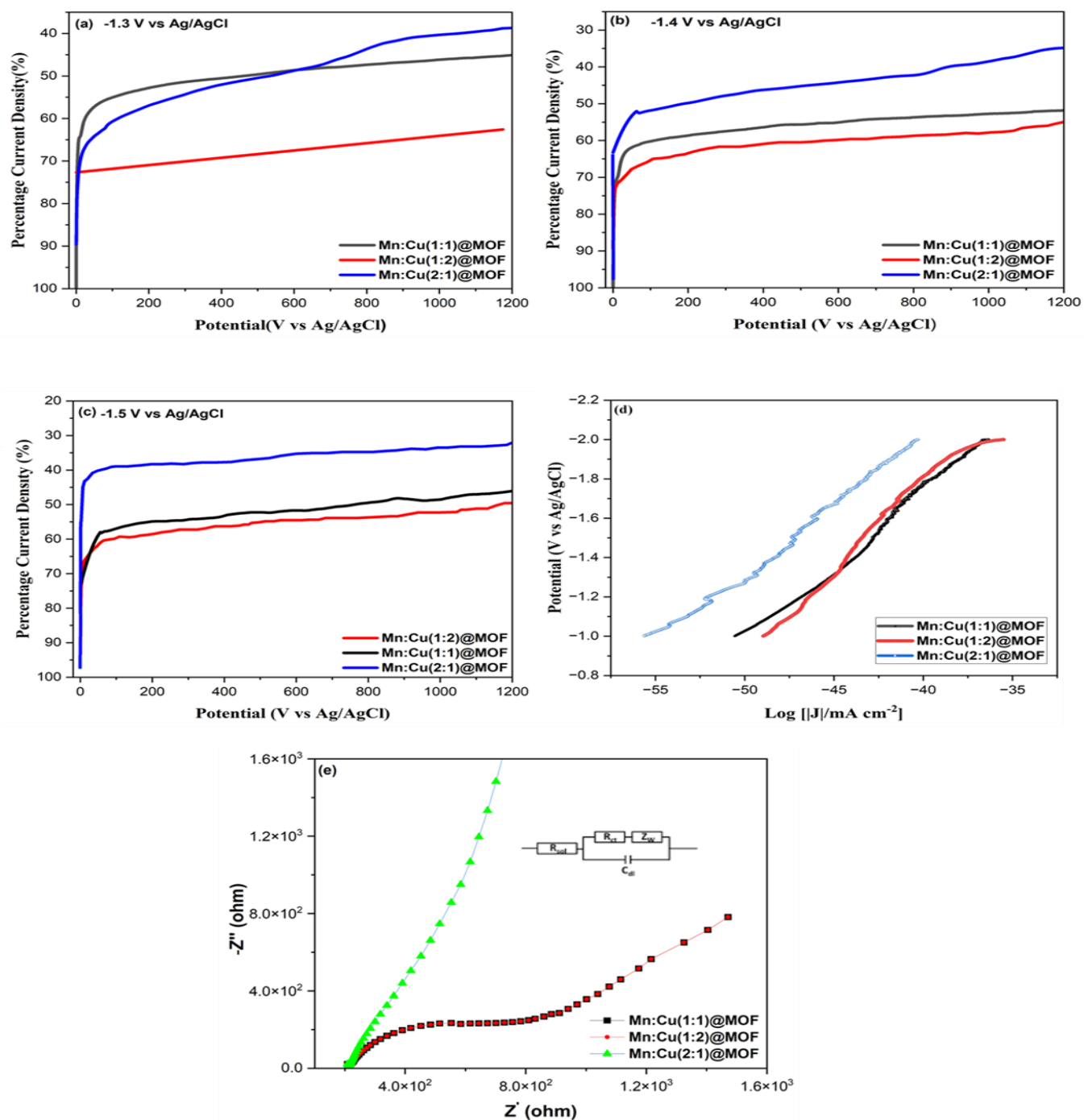
Fig 4.5 Total current density percentage of Mn:Cu(1:1)@MOF, Mn:Cu(1:2)@MOF and Mn:Cu(2:1)@MOF under different constant potentials in CO_2 atmosphere (d) Tafel plots for Mn:Cu(1:1)@MOF, Mn:Cu(1:2)@MOF and Mn:Cu(2:1)@MOF (e) Nyquist curves with corresponding fitting profiles for Mn:Cu(1:2)@MOF, Mn:Cu(1:1)@MOF and Mn:Cu(2:1)@MOF.

Table 4.2 Comparison of reported bi-metallic MOfs and this work

Catalysts	Electrolytes	Applied potential(vs. RHE)	Current Density	Max Faradic Efficiency (FE) of Products	Ref.
Cu_3Sn/Cu_6Sn_5	0.1M $NaHCO_3$	-1 V	-18.9mAcm^{-2}	82% of CO only	[74]
Cu-Ag-10	0.1M $KHCO_3$	-0.74 V	-0.08 mAcm^{-2}	CO=6.5% HCOOH=10% Ethylene=0.72%	[75]
$Cu_1/Pd_{0.3}$	0.5M $KHCO_3$	-0.87 V	-5.1 mAcm^{-2}	55.6% CO only	[76]
C-Cu/In$_2$O$_3$-0.4	0.5M $KHCO_3$	-0.9 V	-12.7 mAcm^{-2}	Syngas 82%	[77]
Cu30%ZIF-8	0.1M $KHCO_3$	-0.56 V	-40 mAcm^{-2}	CO=62% CH$_4$=35%	[63]
Cu-Ni-TiN/C	0.1M $NaHCO_3$	-1.4 V	-15 mAcm^{-2}	CO=19.1% HCOOH=6.7%	[78]
CuBi12-GDE	0.5M $KHCO_3$	-0.9 V	-20 mAcm^{-2}	Methanol=8.6% Ethanol=28.3%	[79]
Co$_3$O$_4$/CuO HNT	0.5M KCl	-0.36 V	-10.5 mAcm^{-2}	98% CO only	[80]
Mn:Cu(1:2)@MOF	0.1M $KHCO_3$	-0.46V	-58 mAcm^{-2}	CH$_4$=54% CO=52%	This Work

Summary

The electrochemical reduction of CO_2 to create methane and CO with selectivity was examined in this study using a novel catalyst termed Mn:Cu (1:2)@MOF. The catalyst was a 2D structure with copper and manganese nanoparticles adhered to its surface. To examine the effectiveness of Mn:Cu@MOFs in the CO_2 reduction process, a range of samples with various manganese and copper ratios were synthesized. This work evaluated the electrochemical reduction of CO_2 to produce methane and CO with selectivity using a novel catalyst called Mn:Cu (1:2)@MOF. The catalyst has copper and manganese nanoparticles attached to its surface and was a 2D structure. A variety of samples with different manganese and copper ratios were synthesized in order to evaluate the efficiency of Mn:Cu@MOFs in the CO_2 reduction process. One interesting finding was that the catalyst's effectiveness increased as the copper content in the catalyst rose. This suggests that copper was essential in improving the CO_2 adsorption, charge transfer, and reaction kinetics, which improved the efficiency of electrochemical reduction (ECR).The results of the study demonstrate the potential of the Mn:Cu (1:2)@MOF catalyst as a practical and efficient CO_2 reduction tool. It is a viable contender for industrial applications targeted at lowering CO_2 emissions due to the selective production of methane and CO as well as the excellent current densities and faradic efficiency. Furthermore, this study opens up promising avenues for further investigation and advancement of sophisticated bi-metallic MOFs as catalysts for effective CO_2 reduction. Researchers can aspire to attain even higher efficiency and selectivity in the electrochemical conversion of CO_2 into useful chemicals by fine-tuning the structure and content of such catalysts. In the end, these developments in catalyst design can considerably aid in the creation of environmentally friendly and sustainable technology to battle climate change and make use of CO_2 as a valuable resource.

References

1.	geopraphic, n. *Non Renewable Energy*. 2023 7/13/2023]; Available from: https://www.nationalgeographic.org/.

2.	nations, u. *The Role of Fossil Fuels in a Sustainable Energy System*. 2023 7/13/2023]; Available from: https://www.un.org/en/.

3.	NASA. *Carbon dioxide*. 2023 7/13/2023]; Available from: https://climate.nasa.gov/vital-signs/carbon-dioxide/

4.	information, N.C.f.e. *Climate at a Glance*. 2023 7/13/23]; Available from: http://www.ncei.noaa.gov/.

5.	Chaabouni, S. and K. Saidi, *The dynamic links between carbon dioxide (CO2) emissions, health spending and GDP growth: A case study for 51 countries.* Environmental research, 2017. **158**: p. 137-144.

6.	data, O.w.i. *Energy Consumption by source. world*. 2023 7/13/2023]; Available from: https://ourworldindata.org/.

7.	IEA. *What is carbon capture, utilisation and storage (CCUS)*. 2023 7/13/2023]; Available from: https://www.iea.org/.

8.	Review, E.I. *Carbon Capture Utilisation and Storage in Clean Energy Transitions*. 2020 7/13/23]; Available from: https://energyindustryreview.com/author/petroleumreview/.

9.	Li, J., et al., *A review of carbon capture and storage project investment and operational decision-making based on bibliometrics.* Energies, 2018. **12**(1): p. 23.

10.	Peter, S.C., *Reduction of CO2 to chemicals and fuels: a solution to global warming and energy crisis.* ACS Energy Letters, 2018. **3**(7): p. 1557-1561.

11.	Barber, J., *Photosynthetic energy conversion: natural and artificial.* Chemical Society Reviews, 2009. **38**(1): p. 185-196.

12.	Wu, J., et al., *CO2 reduction: from the electrochemical to photochemical approach.* Advanced Science, 2017. **4**(11): p. 1700194.

13.	Garg, S., et al., *Advances and challenges in electrochemical CO 2 reduction processes: an engineering and design perspective looking beyond new catalyst materials.* Journal of Materials Chemistry A, 2020. **8**(4): p. 1511-1544.

14.	Zhu, D.D., J.L. Liu, and S.Z. Qiao, *Recent advances in inorganic heterogeneous electrocatalysts for reduction of carbon dioxide.* Advanced materials, 2016. **28**(18): p. 3423-3452.

15. Global Climate Change Indicators | Monitoring References | National Centers for Environmental Information (NCEI), (n.d.). https://www.ncdc.noaa.gov/monitoring-references/faq/indicators.php (accessed December 15, 2020).

16. J. Wu, Y. Huang, W. Ye, Y. Li, CO2 Reduction: From the Electrochemical to Photochemical Approach, Adv. Sci. 4 (2017) 1–29. https://doi.org/10.1002/advs.201700194.

17. F.N. Al-Rowaili, A. Jamal, M.S. Ba Shammakh, A. Rana, A Review on Recent Advances for Electrochemical Reduction of Carbon Dioxide to Methanol Using Metal-Organic Framework (MOF) and Non-MOF Catalysts: Challenges and Future Prospects, ACS Sustain. Chem. Eng. 6 (2018) 15895–15914. https://doi.org/10.1021/acssuschemeng.8b03843.

18. D.S.A. Simakov, Renewable Synthetic Fuels and Chemicals from Carbon Dioxide, Springer International Publishing, Cham, 2017. https://doi.org/10.1007/978-3-319-61112-9.

19. T. Ma, Q. Fan, X. Li, J. Qiu, T. Wu, Z. Sun, Graphene-based materials for electrochemical CO 2 reduction, J. CO2 Util. 30 (2019) 168–182. https://doi.org/10.1016/j.jcou.2019.02.001.

20. A.A. Ensafi, H.A. Alinajafi, B. Rezaei, Pt-modified nitrogen doped reduced graphene oxide: A powerful electrocatalyst for direct CO2 reduction to methanol, J. Electroanal. Chem. 783 (2016) 82–89. https://doi.org/10.1016/j.jelechem.2016.11.04. [1]   F.N. Al-Rowaili, A. Jamal, M.S. Ba Shammakh, A. Rana, A Review on Recent Advances for Electrochemical Reduction of Carbon Dioxide to Methanol Using Metal-Organic Framework (MOF) and Non-MOF Catalysts: Challenges and Future Prospects, ACS Sustain. Chem. Eng. 6 (2018) 15895–15914. https://doi.org/10.1021/acssuschemeng.8b03843.

21. J. Wu, Y. Huang, W. Ye, Y. Li, CO2 Reduction: From the Electrochemical to Photochemical Approach, Adv. Sci. 4 (2017) 1–29. https://doi.org/10.1002/advs.201700194.

22. D. Gao, H. Zhou, J. Wang, S. Miao, F. Yang, G. Wang, J. Wang, X. Bao, Size-Dependent Electrocatalytic Reduction of CO2 over Pd Nanoparticles, J. Am. Chem. Soc. 137 (2015)

4288–4291. https://doi.org/10.1021/jacs.5b00046.

23. R.L. MacHunda, H. Ju, J. Lee, Electrocatalytic reduction of CO2 gas at Sn based gas diffusion electrode, Curr. Appl. Phys. 11 (2011) 986–988. https://doi.org/10.1016/j.cap.2011.01.003.

24. A.S. Agarwal, Y. Zhai, D. Hill, N. Sridhar, The electrochemical reduction of carbon dioxide to formate/formic acid: Engineering and economic feasibility, ChemSusChem. 4 (2011) 1301–1310. https://doi.org/10.1002/cssc.201100220.

25. Y. Chen, M.W. Kanan, Tin oxide dependence of the CO 2 reduction efficiency on tin electrodes and enhanced activity for tin/tin oxide thin-film catalysts, J. Am. Chem. Soc. 134 (2012) 1986–1989. https://doi.org/10.1021/ja2108799.

26. S. Zhang, P. Kang, T.J. Meyer, Nanostructured tin catalysts for selective electrochemical reduction of carbon dioxide to formate, J. Am. Chem. Soc. 136 (2014) 1734–1737. https://doi.org/10.1021/ja4113885.

27. X. Nie, M.R. Esopi, M.J. Janik, A. Asthagiri, Selectivity of CO2 reduction on copper electrodes: The role of the kinetics of elementary steps, Angew. Chemie - Int. Ed. 52 (2013) 2459–2462. https://doi.org/10.1002/anie.201208320.

28. C.W. Li, M.W. Kanan, CO 2 reduction at low overpotential on Cu electrodes resulting from the reduction of thick Cu 2O films, J. Am. Chem. Soc. 134 (2012) 7231–7234. https://doi.org/10.1021/ja3010978.

29. D. Yang, Q. Zhu, C. Chen, H. Liu, Z. Liu, Z. Zhao, X. Zhang, S. Liu, B. Han, Selective electroreduction of carbon dioxide to methanol on copper selenide nanocatalysts, Nat. Commun. 10 (2019) 1–9. https://doi.org/10.1038/s41467-019-08653-9.

30. Y. Huang, A.D. Handoko, P. Hirunsit, B.S. Yeo, Electrochemical Reduction of CO2 Using Copper Single-Crystal Surfaces: Effects of CO∗ Coverage on the Selective Formation of Ethylene, ACS Catal. 7 (2017) 1749–1756. https://doi.org/10.1021/acscatal.6b03147.

31. J. Albo, A. Sáez, J. Solla-Gullón, V. Montiel, A. Irabien, Production of methanol from CO2 electroreduction at Cu2O and Cu2O/ZnO-based electrodes in aqueous solution, Appl. Catal.

B Environ. 176–177 (2015) 709–717. https://doi.org/10.1016/j.apcatb.2015.04.055.

32. Advances in Chemical Conversions for Mitigating Carbon Dioxide - Google Books, (n.d.). https://books.google.com.pk/books?id=9pvLg7VjNTEC&pg=PA225&lpg=PA225&dq=S hoichiro+Ikeda,+Satoshi+Shiozaki,+Junichi+Susuki,+Kaname+Ito,+and+Hidetomo+Noda ,+Electroreduction+of+CO2+using+Cu/Zn+oxides+loaded+gas+diffusion+electrodes,+Ad vances+in+Chemical+Conversions+for+Mitigating+Carbon+Dioxide+Studies+in+Surface +Science+and+Catalysis,+Vol.+114,+1-5&source=bl&ots=0BQrEkHXlC&sig=ACfU3U3pwxWbmmKAqz3MXeXI4klud-iUFQ&hl=en&sa=X&ved=2ahUKEwjqkeHloNrwAhVxoFwKHYffAqoQ6AEwAHoECA IQAw#v=onepage&q=Shoichiro Ikeda%2C Satoshi Shiozaki%2C Junichi Susuki%2C Kaname Ito%2C and Hidetomo Noda%2C Electroreduction of CO2 using Cu%2FZn oxides loaded gas diffusion electrodes%2C Advances in Chemical Conversions for Mitigating Carbon Dioxide Studies in Surface Science. [1]   C. Dhand, N. Dwivedi, X.J. Loh, A.N. Jie Ying, N.K. Verma, R.W. Beuerman, R. Lakshminarayanan, S. Ramakrishna, Methods and strategies for the synthesis of diverse nanoparticles and their applications: A comprehensive overview, RSC Adv. 5 (2015) 105003–105037. https://doi.org/10.1039/c5ra19388e.

33. R. Wang, X. Sun, S. Ould-Chikh, D. Osadchii, F. Bai, F. Kapteijn, J. Gascon, Metal-Organic-Framework-Mediated Nitrogen-Doped Carbon for CO2 Electrochemical Reduction, ACS Appl. Mater. Interfaces. 10 (2018) 14751–14758. https://doi.org/10.1021/acsami.8b02226.

34. S. Goyal, M.S. Shaharun, C.F. Kait, B. Abdullah, Effect of monometallic copper on zeolitic imidazolate framework-8 synthesized by hydrothermal method, J. Phys. Conf. Ser. 1123 (2018). https://doi.org/10.1088/1742-6596/1123/1/012062.

35. Materials Characterization: Introduction to Microscopic and Spectroscopic Methods, 2nd Edition | Wiley, (n.d.). https://www.wiley.com/en-us/Materials+Characterization%3A+Introduction+to+Microscopic+and+Spectroscopic+M ethods%2C+2nd+Edition-p-9783527334636 (accessed May 21, 2021).

36. J.I. Goldstein, D.E. Newbury, P. Echlin, D.C. Joy, C.E. Lyman, E. Lifshin, L. Sawyer, J.R.

Michael, Introduction, in: Scanning Electron Microsc. X-Ray Microanal., Springer US, 2003: pp. 1–20. https://doi.org/10.1007/978-1-4615-0215-9_1.

37. Thermogravimetric Analysis - NETZSCH Thermal Academy, (n.d.). https://www.netzsch-thermal-academy.com/en/advanced-materials-testing/methods/thermogravimetric-analysis/ (accessed May 21, 2021).

38. FTIR Spectroscopy Basics | Thermo Fisher Scientific - PK, (n.d.). https://www.thermofisher.com/pk/en/home/industrial/spectroscopy-elemental-isotope-analysis/spectroscopy-elemental-isotope-analysis-learning-center/molecular-spectroscopy-information/ftir-information/ftir-basics.html (accessed May 21, 2021).

39. Z. Sun, T. Ma, H. Tao, Q. Fan, B. Han, Fundamentals and Challenges of Electrochemical CO_2 Reduction Using Two-Dimensional Materials, Chem. 3 (2017) 560–587. https://doi.org/10.1016/j.chempr.2017.09.009.

40. S. Liang, N. Altaf, L. Huang, Y. Gao, Q. Wang, Electrolytic cell design for electrochemical CO_2 reduction, J. CO2 Util. 35 (2020) 90–105. https://doi.org/10.1016/j.jcou.2019.09.007.

41. N. Elgrishi, K.J. Rountree, B.D. McCarthy, E.S. Rountree, T.T. Eisenhart, J.L. Dempsey, A Practical Beginner's Guide to Cyclic Voltammetry, J. Chem. Educ. 95 (2018) 197–206. https://doi.org/10.1021/acs.jchemed.7b00361.

42. J. Wu, Y. Huang, W. Ye, Y. Li, CO_2 Reduction: From the Electrochemical to Photochemical Approach, Adv. Sci. 4 (2017) 1–29. https://doi.org/10.1002/advs.201700194.

43. F. Lei, W. Liu, Y. Sun, J. Xu, K. Liu, L. Liang, T. Yao, B. Pan, S. Wei, Y. Xie, Metallic tin quantum sheets confined in graphene toward high-efficiency carbon dioxide electroreduction, Nat. Commun. 7 (2016). https://doi.org/10.1038/ncomms12697.

44. F.N. Al-Rowaili, A. Jamal, M.S. Ba Shammakh, A. Rana, A Review on Recent Advances for Electrochemical Reduction of Carbon Dioxide to Methanol Using Metal-Organic Framework (MOF) and Non-MOF Catalysts: Challenges and Future Prospects, ACS Sustain. Chem. Eng. 6 (2018) 15895–15914.

https://doi.org/10.1021/acssuschemeng.8b03843.

45. J. Augustynski, P. Kedzierzawski, B. Jermann, Electrochemical reduction of CO2 at metallic electrodes, Stud. Surf. Sci. Catal. 114 (1998) 107–116. https://doi.org/10.1016/s0167-2991(98)80731-3.

46. Y. Hori, K. Kikuchi, A. Murata, S. Suzuki, of Japan PRODUCTION OF METHANE AND ETHYLENE IN ELECTROCHEMICAL REDUCTION OF CARBON DIOXIDE AT COPPER ELECTRODE IN AQUEOUS HYDROGENCARBONATE SOLUTION, 1986.

47. M. Halmann, Photoelectrochemical reduction of aqueous carbon dioxide on p-type gallium phosphide in liquid junction solar cells [5], Nature. 275 (1978) 115–116. https://doi.org/10.1038/275115a0.

48. Sun, Z., et al., Fundamentals and challenges of electrochemical CO2 reduction using two-dimensional materials. Chem, 2017. 3(4): p. 560-587.

49. Nie, X., et al., Selectivity of CO2 reduction on copper electrodes: the role of the kinetics of elementary steps. Angewandte Chemie, 2013. 125(9): p. 2519-2522.

50. Chen, W., et al., Electrocatalytic CO2 Reduction over Bimetallic Bi-Based Catalysts: A Review. CCS Chemistry, 2023. 5(3): p. 544-567.

51. Pei, Y., H. Zhong, and F. Jin, A brief review of electrocatalytic reduction of CO2—Materials, reaction conditions, and devices. Energy Science & Engineering, 2021. 9(7): p. 1012-1032.

52. Tang, M.T., et al., From electricity to fuels: descriptors for C1 selectivity in electrochemical CO2 reduction. Applied Catalysis B: Environmental, 2020. 279: p. 119384.

53. Zaza, L., K. Rossi, and R. Buonsanti, Well-defined copper-based nanocatalysts for selective electrochemical reduction of CO2 to C2 products. ACS Energy Letters, 2022. 7(4): p. 1284-1291.

54.   Liu, W., et al., Electrochemical CO2 reduction to ethylene by ultrathin CuO nanoplate arrays. Nature communications, 2022. 13(1): p. 1877.

55.   Calle-Vallejo, F. and M.T. Koper, Theoretical considerations on the electroreduction of CO to C2 species on Cu (100) electrodes. Angewandte Chemie, 2013. 125(28): p. 7423-7426.

56.   Xue, Y., et al., MOF-Derived Cu/Bi Bi-metallic Catalyst to Enhance Selectivity Toward Formate for CO2 Electroreduction. ChemElectroChem, 2022. 9(4): p. e202101648.

57.   Ning, H., et al., Cubic Cu2O on nitrogen-doped carbon shell for electrocatalytic CO2 reduction to C2H4. Carbon, 2019. 146.

58.   Wang, L., et al., Integration of ultrafine CuO nanoparticles with two-dimensional MOFs for enhanced electrochemicgal CO2 reduction to ethylene. Chinese Journal of Catalysis, 2022. 43(4): p. 1049-1057.

59.   Zhang, B., et al., Manganese acting as a high-performance heterogeneous electrocatalyst in carbon dioxide reduction. Nature Communications, 2019. 10(1): p. 2980.

60.   Chen, B., et al., Metal-organic-framework-derived bi-metallic sulfide on N, S-codoped porous carbon nanocomposites as multifunctional electrocatalysts. Journal of Power Sources, 2016. 334: p. 112-119.

61.   Chen, L., et al., Bimetallic metal–organic frameworks and their derivatives. Chemical science, 2020. 11(21): p. 5369-5403.

62.   Kitagawa, S., R. Kitaura, and S.i. Noro, Functional porous coordination polymers. Angewandte Chemie International Edition, 2004. 43(18): p. 2334-2375.

63.   Furukawa, H., et al., The chemistry and applications of metal-organic frameworks. Science, 2013. 341(6149): p. 1230444.

64.   Ahmad, A., et al., Cu-doped zeolite imidazole framework (ZIF-8) for effective electrocatalytic CO2 reduction. Journal of CO2 Utilization, 2021. 48: p. 101523.

65.   Li, X., et al., Metal–organic frameworks as a platform for clean energy applications. EnergyChem, 2020. 2(2): p. 100027.

66.   Wang, L., et al., Integration of ultrafine CuO nanoparticles with two-dimensional MOFs for enhanced electrochemical CO2 reduction to ethylene. Chinese Journal of Catalysis, 2022. 43(4): p. 1049-1057.

67.   Mandal, M., K. Chattopadhyay, and S. Bhattacharya, Sunlight mediated photocatalytic reduction of aqueous Cr(Vl) using metal hexacyanoferrate (M = Mn, Ni, Cu and Zn). IOP Conference Series: Materials Science and Engineering, 2021. 1080: p. 012047.

68.   Irikura, K., et al., Electrochemical preparation of Cu/Cu2O-Cu (BDC) metal-organic framework electrodes for photoelectrocatalytic reduction of CO2. Journal of CO2 Utilization, 2020. 42.

69.   Li, J.-R., et al., Insight into the catalytic performance and reaction routes for toluene total oxidation over facilely prepared Mn-Cu bimetallic oxide catalysts. Applied Surface Science, 2021. 550: p. 149179.

70.   Sundriyal, S., S. Mishra, and A. Deep, Study of manganese-1, 4-benzenedicarboxylate metal organic framework electrodes based solid state symmetrical supercapacitor. Energy Procedia, 2019. 158: p. 5817-5824.

71.   Dikio, E.D. and A.M. Farah, Synthesis, characterization and comparative study of copper and zinc metal organic frameworks. Chemical Science Transactions, 2013. 2(4): p. 1386-1394.

72.   Siddig, L.A., et al., Manganese-Based Metal-Organic Frameworks Photocatalysts for Visible Light-Driven Oxidative Coupling of Benzylamine under Atmospheric Oxygen: A Comparative Study. Catalysts, 2023. 13(3): p. 613.

73.   Ramachandran Ph.D, T., et al., Investigation on the electrochemical performance of hausmannite Mn 3 O 4 nanoparticles by ultrasonic irradiation assisted co-precipitation method for supercapacitor electrodes. Journal of Taibah University for Science, 2018. 12: p. 1-9.

74.   Yang, Y., et al., Progress in the mechanisms and materials for CO2 electroreduction toward C2+ products. Acta Phys.-Chim. Sin, 2020. 36(1): p. 1-13.

75.   Wang, J., et al., Heterostructured intermetallic CuSn catalysts: high performance towards the electrochemical reduction of CO 2 to formate. Journal of Materials Chemistry A, 2019. 7(48): p. 27514-27521.

76.   Chang, Z.-Y., et al., Facile synthesis of Cu–Ag bimetallic electrocatalyst with prior C2 products at lower overpotential for CO2 electrochemical reduction. Surfaces and Interfaces, 2017. 6: p. 116-121.

77.   Chen, D., et al., Tailoring the selectivity of bimetallic copper–palladium nanoalloys for electrocatalytic reduction of CO2 to CO. ACS Applied Energy Materials, 2018. 1(2): p. 883-890.

78.   Xie, H., et al., Boosting tunable syngas formation via electrochemical CO2 reduction on Cu/In2O3 core/shell nanoparticles. ACS applied materials & interfaces, 2018. 10(43): p. 36996-37004.

79.   Pan, H. and C.J. Barile, Titanium nitride-supported Cu–Ni bifunctional electrocatalysts for CO 2 reduction and the oxygen evolution reaction. Sustainable Energy & Fuels, 2020. 4(11): p. 5654-5664.

80.   Albo, J., et al., Cu/Bi metal-organic framework-based systems for an enhanced electrochemical transformation of CO2 to alcohols. Journal of CO2 Utilization, 2019. 33: p. 157-165.

81.   Cheng, Z., et al., Construction of cobalt-copper bimetallic oxide heterogeneous nanotubes for high-efficient and low-overpotential electrochemical CO2 reduction. J. Energy Chem., 2021. 54: p. 1-6.

List of Publications

1. Umar Raza, Naseem Iqbal, Awais Ahmad**. "Development of Mn/Cu Bi-metallic MOF for electrochemical CO$_2$ reduction into valuable products." Journal Environmental Chemical Engineeringhttps://www.sciencedirect.com/journal/journal-of-environmental-chemical-engineering, Elsevier, July 2023. (Submitted).**